I.D. FOS Research E.E.I.G.
(European Economic Interest Grouping)

DBE TECHNOLOGY GmbH

Operational Safety Monitoring with Fiber Optic Sensing Systems

Final Report Vol. I - Summary and Evaluation -

Authors: Michael Jobmann[1]
Johan Vlekken[2]
Marc R-H Voet[2]

[1]DBE TECHNOLOGY GmbH, Eschenstraße 55, D-31224 Peine, Germany
[2]I.D. FOS Research E.E.I.G., Cipalstraat 12, B-2440 Geel, Belgium

Peine, June 2005

This report consists of three volumes:

Volume I: Summary and Evaluation (main report)

Volume II Technical Details

Volume III Standard and Qualification Document

The reported research work has been funded by the Federal Ministry of Economics and Labour (BMWA = Bundesministerium für Wirtschaft und Arbeit) under the contract No FKZ 02E 9249. However, the authors are responsible for all the content.

Table of contents

Summary

The present report deals with the research and development activities performed between 01.02.2000 and 31.12.2004 in the framework of the research project:

"Development and Testing of Fiber Optic Monitoring Systems Devoted to Operational Safety in Nuclear Waste Disposal Sites. "

funded by German Federal Ministry of Education, Science Research and Technology as well as the Ministry of Economics and Labor in Germany. The activities performed within this project can be divided in three categories:

- The first category contains the activities related to the development and optimization of new types of sensors based on FBG technology as well as intensity based technology. This has resulted in a new spectrum of sensors which are running now in new demonstration sites or which are becoming in the final stage of development.
- The second category contains the research efforts with respect to the interrogation systems. The goal of this system was to enhance the performances and reliability of the existing interrogation system.
- The third category deals with field installations at different sites allowing detailed evaluation of the sensors as well as the complete sensing system under realistic monitoring conditions.

First of all, extensive research has been performed to new sensor designs. The following sensors have been developed from scratch or improved by a redesign of the sensor design or by applying new processing algorithms:

1. A distributed temperature cable has been developed for high temperature applications. The cable exists of a carbon reinforced optical fiber containing different Fiber Bragg Gratings (FBG.)
2. A high resolution strain sensor has been developed for measuring fissurization.
3. A high resolution deformation cable has been taken under development. In opposition to the already existing strain deformation cable, this new cable makes use of high resolution strain sensors. Due to planned applications in high temperature environments special attention has been addressed with respect to the thermal expansion effects of the cable by using special carbon materials with a very low thermal expansion coefficient.
4. New pore water pressure sensors as well as total pressure sensors together with corrosion resistant housings have been developed. The sensors are qualified to measure pressures up to 150 bar within a temperature range from 0 up to 180°C. This research did also require the development of the necessary calibration systems, a fatigue testing system and a new calibration algorithm.
5. A new calibration procedure for the water leakage sensor has been developed. This new calibration method takes also the thermal expansion of the housing into account and results into a much better response behavior.
6. Two new designs for the hydrogen sensor have been developed and tested. One of the two sensors did show an excellent sensitivity but improvements are required to speed up the response time. This has resulted into the development of a third new design which is still under development.

7. An intensity based pH sensor has been developed and an in-situ test of the sensor has been performed at the Königstein mine. The pH sensor did show an excellent short term behavior. For the long term measurements significant drift effects could be observed. Therefore, some more research is required to improve the sensor for long term monitoring applications.

Besides the developments on sensor level, a lot of research has been performed with respect to the interrogation system. The interrogation system, developed under a former project, has been completely redesigned. Due to new developments in the telecommunication market the system performances and cost effectivity could drastically be improved by integrating new types of components. This has been carried out and the necessary software components have been developed.

- Furthermore, several in-situ tests have been performed at different sites in Germany, Switzerland and Sweden.

Finally, a draft of a

"*Standard and qualification document for fiber optic sensing systems to be applied at nuclear waste repository sites*"

has been written. The intention of the document is to provide an internationally acceptable standard for general requirements to control, fiber optical sensing systems by defining minimum requirements for design, materials, fabrication, installation, testing, commissioning, operation, maintenance, re-qualification and abandonment. This document is a first step in bringing the fiber optic sensing systems to a commercialization level.

In general, the development of fiber optic sensors and interrogation systems as well as the laboratory and in-situ measurements yield very promising results. Sufficient conclusions can be drawn due to the fact that a broad comparison with conventional sensors was possible resulting in a good correspondence between conventional and fiber optical sensors. The reliability of fiber optic systems has thus been proven.

As a general result, it can be stated that fiber optic monitoring systems devoted to operational safety at nuclear waste disposal sites is becoming a very interesting alternative for the conventional electrical sensing systems.

1. Introduction and objectives

For several years, fiber-optic sensing devices had been used for straightforward on/off monitoring functions such as presence and position detection. Recently, they are receiving increasing attention as they offer a novel, exciting technology for a multitude of sensing applications. In the deep geological environment most physical properties, and thus most parameters important to safety, can be measured by using fiber-optic technology. Due to this, DBE TECHNOLOGY is developing sensing systems based on this technology as the basis for monitoring systems at final repositories [1], [2], [3].

The targeted scope of the work under this research project is the development and testing of fiber optic monitoring systems devoted to operational safety at nuclear waste disposal sites.

The objectives of this project have been focused on the achievement of a long term monitoring system. Such a system has to measure physical parameters for thermo-hydro-mechanical monitoring of structures within final repositories (water ingress, temperature evolution, strain and displacements, pressure) as well as the contents of harmful gases for operational safety purposes. The system also has to carry the gathered information through a network from every point of the monitored repository to a central monitoring station. In this station, information processing has finally to be carried out to ensure a safety operation of the repository.

The feasibility of using such a sensing system has already be shown in previous R&D projects [2] [4]. Some first sensors and interrogation systems have been developed under these projects and demonstrated in field installations in the Asse salt mine and the Konrad mine in Germany.

Within this project, previous developments have been continued and extended to more different sensors and better reliable systems. The targeted main objectives of the project are:

1. Development of new sensors addressing the agreed parameters such as: pH, hydrogen, distributed temperature, pore water pressure, total pressure, fissurization, and high resolution deformation effects.
2. Further development and improvement of the interrogation systems for monitoring of complex large scale sensing networks.
3. Extending the evaluation results of the behavior of the fiber optical monitoring systems in real field installations.

2. Scientific and technical state-of-the-art

At the beginning of this project, the authors had already successfully finalized two projects concerning research and development of long term fiber optical monitoring system to be applied at final repositories for heat generating radioactive waste [1], [2]. The sensors were mainly based on the Fiber Bragg Grating technology [5], [6]. Three different sensors (transduction mechanisms) had been developed for measuring temperature, humidity and displacement. Based on the displacement cell different configurations had been designed for measuring deformations in boreholes. This has been resulted into the strain and anchor displacement cable. Furthermore, some basic research had been carried out for measuring pH and hydrogen concentrations.

Besides the sensor part, a prototype of an interrogation system and monitoring software for complex sensing networks had been developed. However, this system was based on the state of the art of that time. New developments in the telecommunication market did open new and more cost effective possibilities which were not yet integrated.

Finally, some basic field experience was present. Two mines had already been installed: the Morsleben mine and the Asse salt Mine. These field tests allowed to have some very important feedback from the sensing system.

All these developments and activities resulted into new insights and ideas that have been validated in the framework of this project. This has resulted in an extended portfolio of fiber optical sensors based on the FBG technology and a complete new interrogation system.

3. Project follow up

The work of the project has been performed in close cooperation with the company I.D. FOS Research in Belgium which is specialized on the development of fiber optic sensing systems for engineering applications.

At the beginning sensor specifications have been defined to meet the requirements for an application at underground laboratories, mines and final repositories. Afterwards the fiber optic sensing systems have been designed and fabricated and the laboratory test phases have been started.

In parallel to the work on the sensor level several improvements have been performed with respect to the interrogation system. After successful laboratory tests and calibration both the new sensors and the interrogation systems have installed at different underground sites to gain experience on their behavior under real conditions.

The results of the project are compiled in 3 reports

Volume I Summary and Evaluation
Volume II Technical Details
Volume III Standard and Qualification Document

Meanwhile, parts of the project results have been published in national and international journals [3], [7], [8], [9].

Necessary literature studies have been performed using the “Technische Informationsbibliothek der Universität Hannover (TIB)”, the library of the “Bundesanstalt für Geowissenschaften und Rohstoffe Hannover (BGR)” and the library of the University of Brussels.

4. Sensor development

4.1. Carbon protected temperature chain

A special type of a temperature cable has been developed. Since temperature cables will for example directly be installed in a borehole or in an engineered barrier system with different mechanical loads, a good protection mechanism of the optical fiber is requested. The ideal protection should fulfill the following criteria points:

1. low weight
2. flexible
3. small diameter
4. protection against harsh environments (corrosion)
5. protection against high tension loads
7. easy fabrication process
8. cause no delay in response time

As can be noticed, these criteria are not all fulfilled with standard protection systems such as the steel reinforced and armored outdoor and sub sea cables. Therefore, the development of a special temperature cable was started. The current research effort involved reinforcing the FBG sensor arrays with carbon using a standard pultrusion process. Cable design and test system are shown in Fig. 4.1 and 4.2. This design has the advantage that the carbon fibers give a very good protection against high tension loads without the need of over sizing the weight and diameter of the final cable. Furthermore, the carbon shield gives a very good protection against corrosion and can be made watertight.

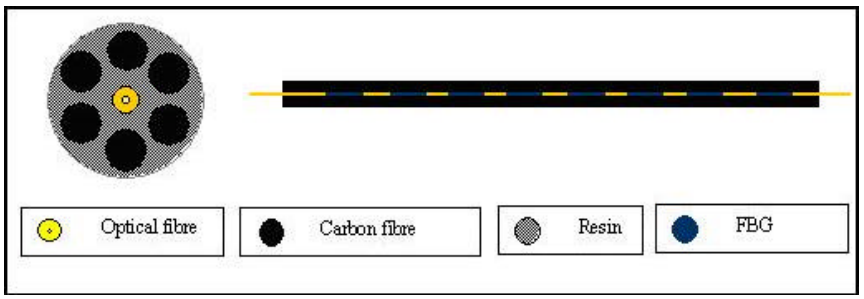

Fig. 4.1:

Design of temperature cable

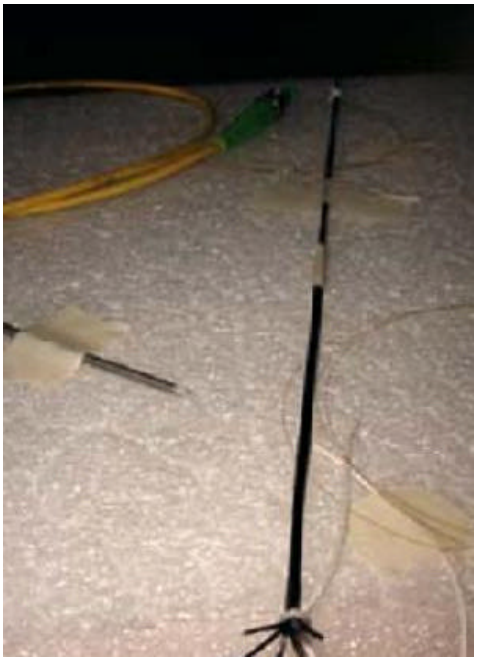

Fig. 4.2: Test system of temperature cable.

The pultruded carbon reinforced sensing fiber has been produced using a standard pultrusion process. Fig. 4.3 shows a schematic diagram of the process. Six carbon fibers with a diameter of 700 µm and one polyamide coated glass fiber with a diameter of 155 µm are pulled through a resin impregnation bath (Epoxy resin). The glass fiber is positioned at the center and contains one FBG with a nominal wavelength of 1531.8 nm at 20°C. Subsequently, the fibers go through a shaping die of 2 mm diameter and are subsequently cured to harden out the resin. The resulting part is a 2 mm diameter carbon reinforced sensing fiber. This production process can be fully automated and allows the fabrication of very long lengths, up to several km.

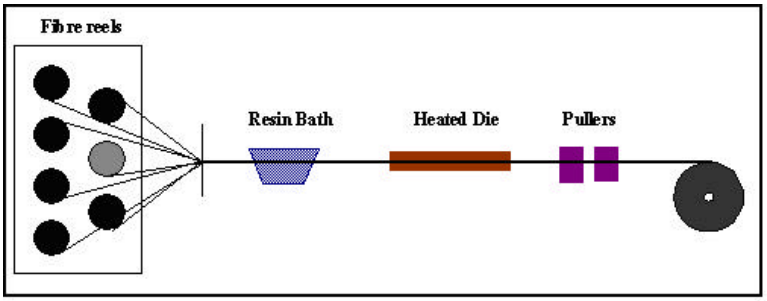

Fig. 4.3: Schematic overview of pultrusion process

In order to characterize the temperature cable, three different experiments were performed. In a first experiment, a temperature calibration has been performed yielding a good linear relation. The sensitivity is equal to 8.5 pm/°C. This is lower than the sensitivity of the naked FBG which has been measured to be equal to 9.8 pm/°C. This can be explained by the negative thermal expansion coefficient of the carbon fiber. Due to the increasing temperature, a negative strain is applied on the FBG by the carbon fibers resulting in a decrease of the temperature sensitivity. This change in temperature sensitivity is determined by the type of reinforced fibers and the used resin. As a consequence, by choosing other materials, the temperature sensitivity can be increased or decreased dependent on the requested specifications. For example, using a mix of carbon and glass as reinforced fiber will increase the temperature sensitivity.

In a second experiment the temperature response time of the temperature cable has been investigated. The carbon reinforced FBG shows a similar temperature response as the naked FBG, so it can be concluded that almost no delay is induced by the carbon reinforcement. Based on the previous two results it is proven that the temperature cable is suitable for temperature measurements.

Finally, in a third experiment, some strain tests were applied. The temperature cable was put under different load levels, ranging from 0 up to 5 kg and back from 5 to 0 kg. A good linear behavior between wavelength and load could be observed with a sensitivity of 24 pm/kg. Since the sensitivity of the naked FBG is around 10 nm/kg, this indicates that the reinforcement is working very well. Almost no hysteresis has been observed. The maximum load level of 5 kg has been limited by the experimental set-up and not by the cable itself. The cable can sustain much higher load levels, dependent on the type of carbon fibers, resin, and adaptive diameter. The current technical data as well as a schematic network configuration of a temperature sensing system is shown on figure 4.4. A first field test of the carbon protected temperature chain is planned at the Mont Terri site in Switzerland in the beginning of 2004.

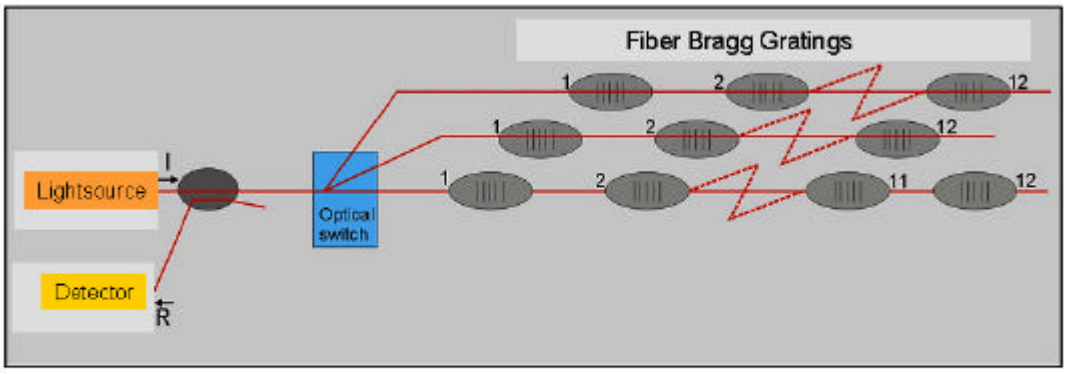

Cable length:	max. 10 km	Resolution:	0.03 K
Cable diameter:	2-10 mm	Accuracy:	0.25 K
Sensors per line:	max. 24	Range:	0 – 100 °C (Acrylat-Fiber) 0 – 180 °C (Polyamide-Fiber)

Fig. 4.4: Schematic configuration of a temperature sensing network

4.2. Fissurometer (mountable strain sensor)

The existing one dimensional mountable strain sensor has been further developed for high resolution applications, for example at the Morsleben site. Compared to existing displacement sensors which for example have been used at the Konrad site, this sensor has the advantage of a much higher sensitivity yielding in a better resolution. In Figure 4.5 and Fig 4.6 the design and a photo of the high sensitive fissurometer is shown.

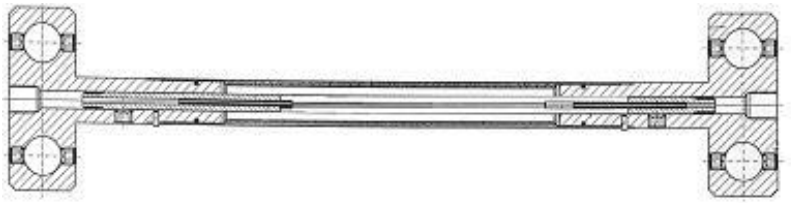

Fig. 4.5: Design of fissurometer

Fig. 4.6: Photo of fissurometer

The fissurometer consists of two anchoring pieces and a fiber with a FBG stretched in between. Both points are connected using a metallic tube in order to protect the fiber. The sensor is designed in such a way that the metallic tube can slide over the short inner tubes of the anchoring points. As a consequence, in opposite to the strain sensor, the metallic tube is not inducing a counter force when the sensor becomes longer. This makes the fixation of the sensor on the structure less critical and the measurements more accurate.

A second difference to the strain sensor is the mounting mechanism of the fissurometer. The fiber containing the FBG is not stretched during the assemblage of the sensor. The strain offset is put on the fiber during the mounting of the sensor. The anchoring holes are larger than the bolts used to fix the sensor to the structure. In order to fix the sensor tightly, the bolts are fixed in the holes by imbus screws located at each side of the hole. By tightening first the outer imbus screws, a strain offset can be put in a controlled manner on the FBG. The advantage of this system is that the sensor can easily be reset for further measurements when the displacement has reached its maximum range. Finally, the fissurometer has a second FBG in an unstressed state for taking into account the temperature sensitivity of the strain-FBG.

The sensitivity of the fissurometer is determined by the length of the free fiber (L_f) and the sensitivity to strain of the strain-FBG (b):

$$S = (b/L_f) \cdot 10^6 \qquad (4.1)$$

With

S = sensitivity [nm/mm]
b = strain sensitivity of the FBG [nm/µm]
L_f = free length of the stretched fiber [mm]

In order to determine the sensitivity factor experimentally, a calibration bench was constructed. The calibration bench allows to displace one of the end points on a controlled manner while keeping the other end point fixed. The displacement is measured using a conventional displacement meter.

A test system of the high sensitive fissurometer was built and characterized. Taking into account the length of the free fiber of 100 mm and the strain sensitivity of the FBG of 1.2 nm/με (με = 10^{-6} mm/m) a sensitivity of 12 nm/mm was expected. The results of the calibration yield a sensitivity factor of 11.857 nm/mm which is in good correspondence with the theoretical value. Furthermore, a good linearity was observed (R^2 = 0.9998). Notice that the sensitivity can further be increased by decreasing the length of the stretched fiber.

Fig. 4.7: Installation of a fiber optic fissurometer at the Morsleben site

An in-situ test of three fiber optic fissurometer has been performed at the Morsleben repository. The fissurometers have been installed at different fissures in a large opening on the first level in the vicinity of conventional systems for the purpose of comparison. The measurement results are shown on figure 4.8. All sensors are indicating some variations in fissure opening. The resolution of the conventional fissurometers is ± 10 µm and for the optical system ± 0.1 µm which is about three orders of magnitude higher. Considering the different resolution abilities a good correspondence can be stated. The measurement trends are characterized by both types of sensors in a similar way except for the end of the measurement period where the optical system indicates a smaller displacement as the conventional system. It is assumed that this is due to the fact that the compared fissurometers are not located exactly at the same position. Discontinuities of fissure openings (see fig 4.7) are assumed to be the reason for small differences in fissure movement.

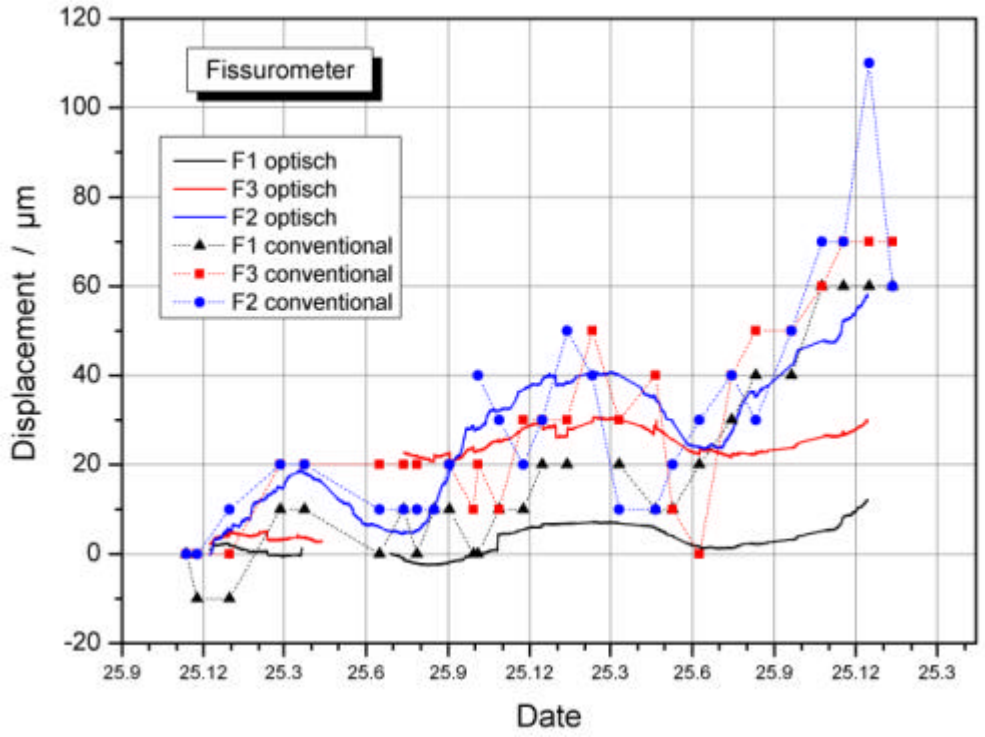

Fig. 4.8: Measurement results of fiber optic and conventional fissurometers at the Morsleben site

At the end of the measurement period the fissurometers have been dismantled for laboratory investigation purposes to check the sensor behavior after 2 years of underground working in a salt environment. Fig. 4.9 shows the recalibration of the fissurometer SN01102503 compared with the calibration curve before installation. As can be observed a good linear correlation still exists. Furthermore, the sensitivity coefficients are very much the same: 7.6147 and 7.5894 respectively. The offset however cannot be compared, this is due to the fact that the calibration measurement is a relative measurement method. However, a change in offset would be expected if the fibre fixation is not working well resulting in a longer free fibre inside the sensor. If this would have been happened, this would also change the sensitivity coefficient that is not the case. It therefore can be assumed that no significant offset change has been taken place. For the other two fissurometers, similar results have been obtained. It therefore can be concluded that no remarkable ageing effect has been taken place for these sensors.

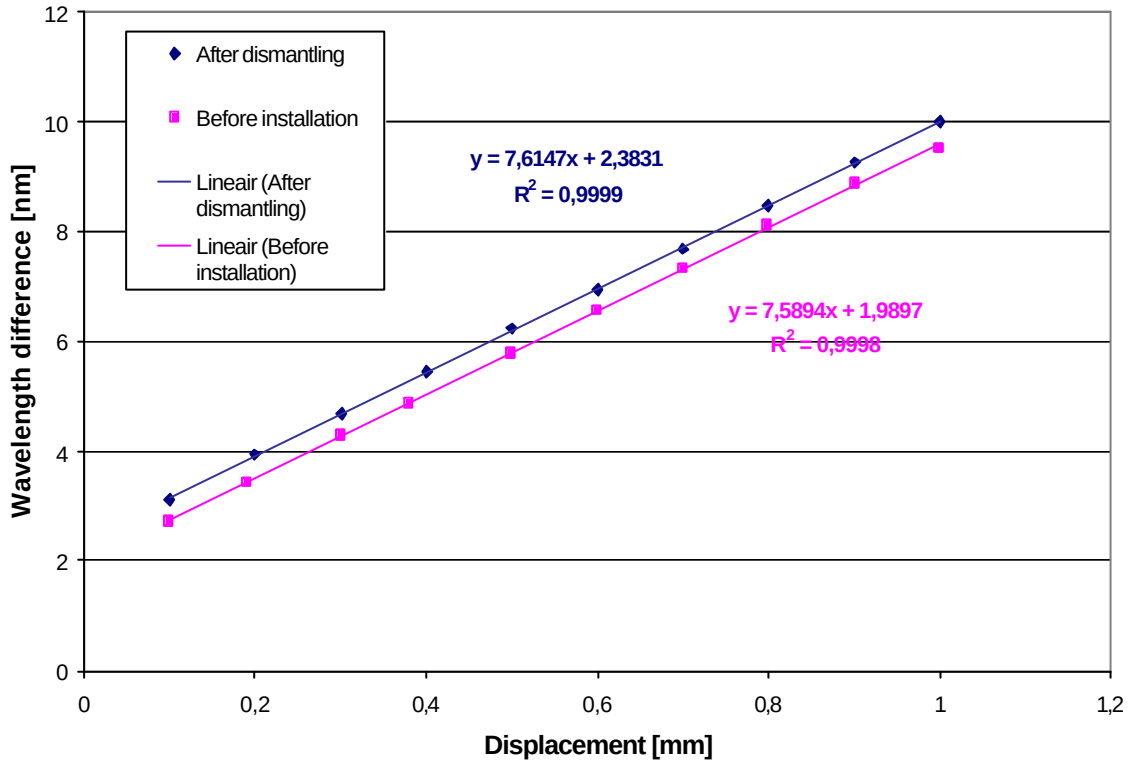

Fig. 4.9: Comparison of sensor calibration before and after the in-situ test

4.3. High resolution strain cable

A new type of strain cable has been developed especially for high resolution measurement purposes. The sensor developed in a previous project as well as the connection mechanism has been redesigned.

4.3.1. The strain cable sensor

A schematic drawing of the opto-mechanical cell is shown in Figure 4.10. The cell consists of a metallic tube with a fixation point on each end. Between both fixation points a fiber containing a Fiber Bragg Grating (FBG) is stretched. This FBG is called the strain-FBG. One fixation

point of the cell can slide when it is pulled to the outward direction. As a consequence the FBG becomes more or less strained resulting in a wavelength shift. Another parameter influencing the wavelength shift is the temperature. A sensitivity of 10.46 pm/°C was expected. In order to compensate for these influences, a second FBG which remains all the time unstrained, is used. This FBG is called the temperature-FBG and allows for monitoring the temperature.

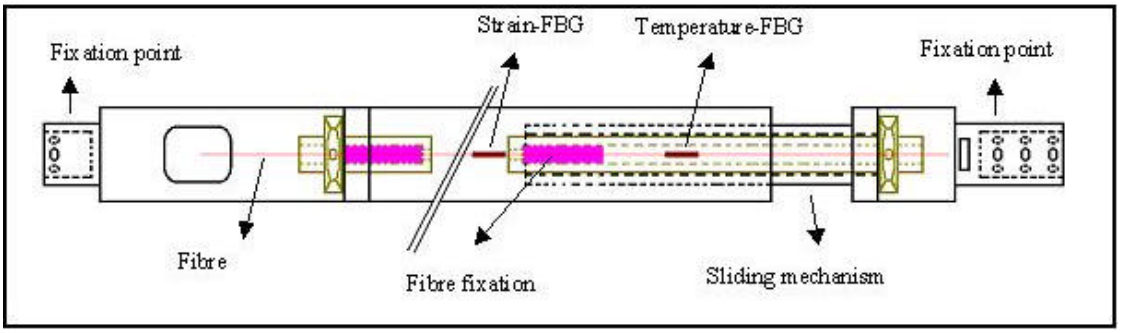

Fig. 4.10: Schematic drawing of an opto-mechanical cell

The relative displacement (Δd) of the sliding fixation point can be calculated using the wavelength shift of the strain-FBG ($\Delta\lambda$), the strain sensitivity of the grating (1.2 pm/με) and the length of the fiber under stress (L_{FBG}):

$$\Delta d = \Delta\lambda \bullet L_{FBG} \bullet 10^{-6} / 1.2 \qquad (4.2)$$

with Δd and L_{FBG} expressed in mm and $\Delta\lambda$ expressed in pm.

The resolution of the sensor is mainly defined by the resolution of the interrogation unit and is as function of the length of the fiber under stress (L_{FBG}). The resolution of the interrogation unit is typically 1 pm. This corresponds to a displacement resolution (d_{res}) of the opto-mechanical cell of:

$$d_{res} = L_{FBG} \bullet 10^{-6} / 1.2 \qquad (4.3)$$

The range of the sensor is defined by the maximum strain that the strain-FBG can sustain. Special fabricated FBGs are used which can sustain a strain of up to 5%. In order to assure a reliable working of the sensor, only the half of the maximum strain level is used (2.5 %). This corresponds to a strain range of:

$$d_{range} = LFBG \bullet 0.025 \qquad (4.4)$$

Based on equation 4.2 and 4.3 it can be calculated that the resolution is equal to 3.33 10^{-4} of the full range. This type of sensor can be customized very easily depending on the requirements requested by the application. L_{FBG} can be chosen between 0.1 and 1 m. Figure 4.11 shows a photo of a strain sensor with L_{FBG} around 680 mm. The cell was calibrated using a calibration set-up especially designed for this type of sensor. A very good linear relation was observed (R^2 =1) and almost no hysteresis is present.

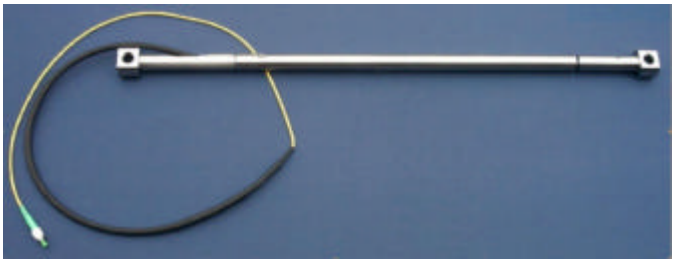

Fig. 4.11: Photo of a small strain sensing element

4.3.2. The strain cable connection mechanism

This type of strain cable has been developed for an installation in boreholes to measure the deformation within different borehole intervals for rock deformation evaluation. In order to transfer the displacement between two packers (fixation in a borehole) to the opto-mechanical cell, carbon tubes were used. The tubes do have an outer diameter of 22 mm, an inner diameter of 18 mm and a low thermal expansion coefficient in order to minimize the displacement errors caused by temperature changes of the environment.

Fig. 4.12: Connection piece for carbon rods and dummy packer

The carbon tubes have a length of 3 m. In order to cover longer distances between two packers, connection rods made of stainless steel are used (Fig. 4.12). At both sides of the connection rods, the carbon tubes are slide to the center and screwed using 6 bolts each. In order to circumvent a bend of the carbon tube due to the weight of the stainless steel rod, a dummy packer in PVC is positioned at the center to guide the pressure and signal tubes of the strain cable to keep the tubes in the center of the borehole.

4.3.3. Adaptation of packers

In order to obtain a high resolution strain cable, the knee coupling fixation mechanism between the rods and the packers of a former strain cable being developed earlier for an application at the Konrad site [2] has been changed by a similar principle as the connection piece (Fig. 4.13). The carbon tube is fixed using six bolts.

Fig. 4.13: Carbon - Packer fixation mechanism

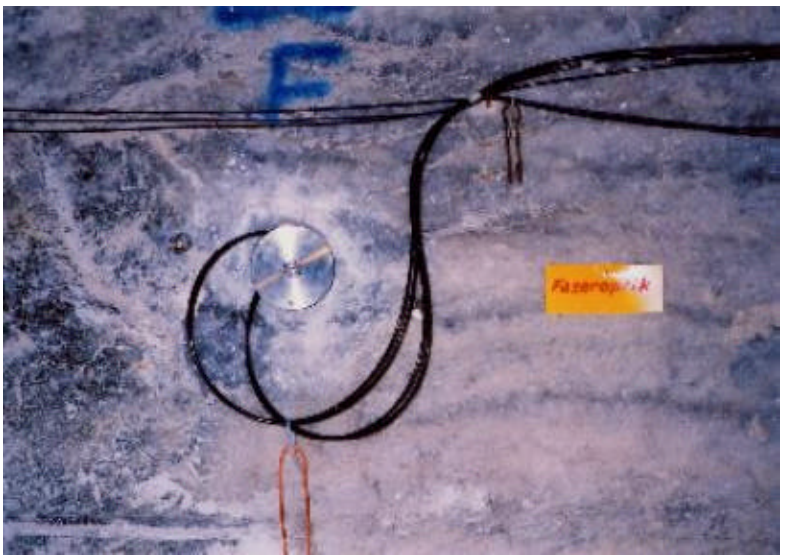

In-situ test measurements have been performed at the Morsleben site for about 2 years. A strain cable having four sensing elements has been installed in a borehole (Fig. 4.14)

Fig. 4.14: Front plate of the installed strain cable with out coming fibers for deformation and temperature measurements

Figure 4.15 shows results of the strain cable measurements at the Morsleben site. Interval 1 and 2 show an increase in distance between the different packers indicating a convergence into the mine opening beginning at April 2004. This is due to backfilling activities in the mine openings accompanied by a temperature increase (lower graph in figure 4.15). One interval has not been recorded anymore since 20 November 2003. This is due to a too low signal. In addition sliding micrometer measurements from an adjacent borehole are plotted into the upper graph. These measurements have been recalculated to obtain comparable interval displacements. A comparison yielded diverse results. The displacements obtained from interval 2 fit well with the sliding micrometer measurements from the second borehole. The increase of the relative displacements of interval 1 during the phase of temperature increase is significantly higher than the sliding micrometer measurements. In interval 3 no significant reaction has been recorded. The latter can be attributed to the spring mechanism. The higher deformation during the phase of temperature increase was assumed to be due to the uncompensated thermal expansion of the carbon cable that was expected to be small enough.

Lessons learned: The spring mechanism has to be improved especially for serial configuration of interval connections. The temperature effect on the carbon extension cable has to be compensated for. These “learned lessons” have been used to improve the new extensometer configurations recently applied at the Mont Terri and Bure URL in Switzerland and France in the framework of another research project. Within these configurations damping effects are excluded and additional FBGs for temperature measurements have been implemented in each individual carbon cable to compensate for temperature effects [29].

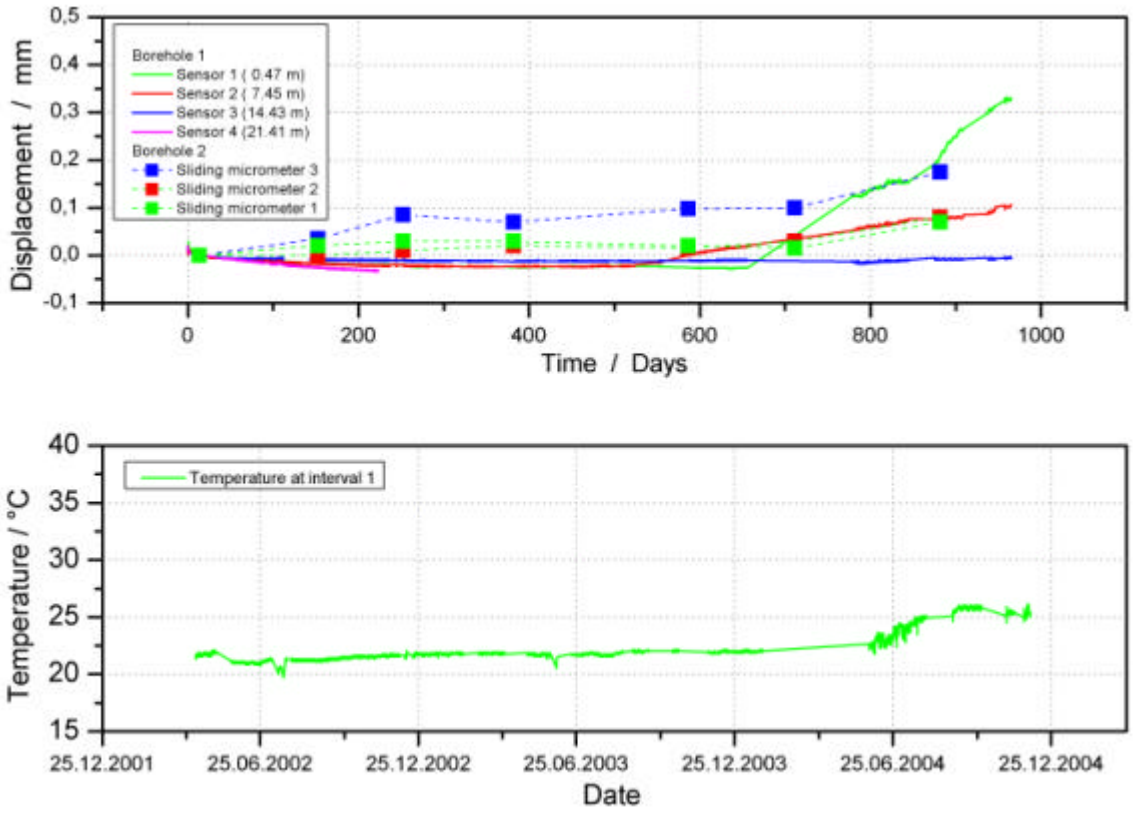

Fig. 4.15: Results of the strain cable measurements

Based on the achieved developments and learned lessons different types of sensing elements listed on table 4.1 can be made available depending on the kind of application. Each interval in a borehole can be equipped with a different type of sensing element, thus making use of different dynamic ranges and resolutions to optimize the measurement results with regard to the expected deformations.

Type	Range	Resolution	Typical Accuracy	Hysteresis
SD-II FOS 2	2 mm	0.084 µm	0.84 µm	< 0.1% F.S.
SD-II FOS 10	10 mm	0.42 µm	4.2 µm	< 0.1% F.S.
SD-II FOS 20	20 mm	0.84 µm	8.4 µm	< 0.1% F.S.

Tab. 4.1: Typical types of strain cable sensing elements

4.4. Development of testing system for pressure cells

In parallel to the development of pressure and porewater presser sensors a laboratory test system for pressure cells had to be established. Thus, a system for automatic testing of pressure cells has been developed to measure the behavior of pressure membranes as a transduction mechanism to the optical fibers. The developed system allows to put the sensor sequentially under 5 different pressure levels. After each sequence the pressure will be released and the next sequence will start. During the cycling, the system measures and saves the optical wavelengths together with the corresponding pressure levels. The system consists of 4 main parts: pressure board, electronic module, Laptop + software and FBG-IS.

The pressure board is shown in Fig. 4.16. A high pressure level, produced by a compressor will serve as input on this pressure board (5). Before going down in the circuit, the inlet passes a double overpressure protection valve (1). This allows limiting the pressure to the maximum allowed value that the membrane can sustain in order to avoid plastic deformation of the membrane. Under the protection valves, five other pressure valves are used to set the individual pressure levels for the fatigue testing. After each pressure valve, a relay controlled ON/OFF valve is placed (2). The different relays are controlled using the software and the electronic module. Each ON/OFF valve will sequentially be opened and the corresponding pressure level at that place will pass via the output line (4) to the sensor (sensor is connected with the right side of the output line. After one complete sequence is finished, the ON/OFF valve (3) will be activated resulting in a pressure release of the sensor.

The electronic module consist of different ON/OFF relays controlled by a LabVIEW [10], [11], [12] program and a Data Acquisition Card (DIO 24). The complete system is controlled using a LabVIEW program.

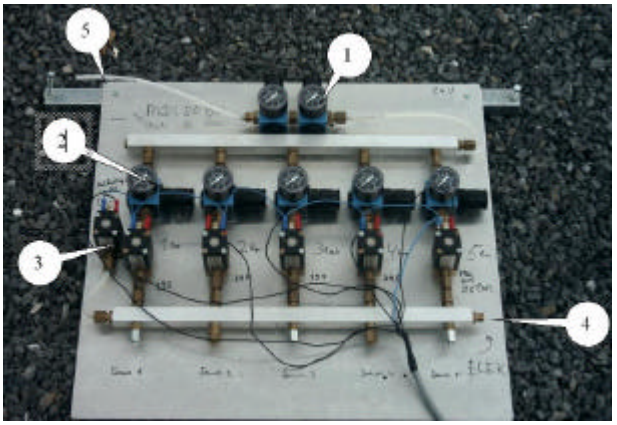

Fig. 4.16: Pressure board

4.5. Porewater pressure sensor

A new design for a porewater pressure sensor has been build. The sensor is designed for measuring pressures up to 50 bar at temperatures up to 180°C. These specifications where required for example in the field experiments at Äspö. The sensor has been designed such that the dimension is kept as small as possible. Due to high temperature levels a new calibration method and system set-up has been developed.

4.5.1. Sensor design

The measurement principle of the fiber optical pressure cells is shown in Fig. 4.17. The membrane pressure sensor hosts a mechanism that aims to allow the dimensioning of the sensor and especially to improve its sensitivity. The mechanism consists in a circular membrane closing at one end the pressure sensing cell. The pressure to be measured is applied on the front of the membrane.

An optical fiber hosting two FBGs is glued in two capillaries. The pressure sensing FBG is glued between the first capillary and the second capillary whereas the temperature compensating FBG is located in the second capillary. The fiber pigtail is spliced to the temperature compensating FBG. At the output of the first capillary the optical fiber is beveled.

Fig. 4.17: Basic design of the membrane pressure sensor

The first capillary is fixed onto the membrane, behind the membrane, at the center and is perpendicular to the plane of the membrane. The second capillary is fixed at the end of the holder which is screwed to and behind the membrane.

The pressure FBG is pre-stretched between the center of the circular membrane and the holder. The pressure to be measured is applied onto the membrane and bends it slightly resulting in a displacement of its center. The pressure FBG is thus released by increasing the pressure while it is stretched by decreasing the pressure. The FBG spectral shift $\Delta\lambda_{FBG}$ is proportional to the pressure difference $P - P_{atm}$ according to equation (4.5) :

$$\Delta\lambda_{FBG} = b_{FBG} \cdot \Delta\varepsilon_{FBG} = b_{FBG} \cdot \frac{\Delta d_{memb}(th_{memb}; Y_{memb}; \sigma_{memb}; (P - P_{atm}))}{L_{0FBG}} \qquad (4.5)$$

Δd_{memb} : displacement of the centre of the membrane
b_{FBG} : FBG strain sensitivity
$L_{0\,FBG}$: FBG length at rest
th_{memb} : membrane thickness
Y_{memb} : membrane Young' modulus
σ_{memb} : membrane Poisson ratio
P_{atm}: Atmospheric pressure

The displacement of the center of the membrane is given by equation (4.6) with R_{memb} the radius of the membrane.

$$\Delta d_{memb} = \alpha R_{memb}^{3} \sqrt{\frac{(P - P_{atm}) R_{memb}}{Y_{memb}\ th_{memb}}} \qquad (4.6)$$

with:

$$\alpha = \sqrt[3]{\frac{6615(\sigma_{memb}^{2} - 1)}{2\ (2791\sigma_{memb}^{2} - 4250\sigma_{memb} - 7505)}} \qquad (4.7)$$

Based on this principle a new design has been made. The new porewater pressure sensor has a length of 260 mm and a maximal outer diameter of 30 mm. The dimensions of the new porewater pressure sensor are shown in Figure 4.18.

The sensor has been created in stainless steel as well as titanium. Titanium has the advantage that it is much more resistant against corrosion. The disadvantage is however the price aspect due to the higher material cost and the more extensive labor required for this material.

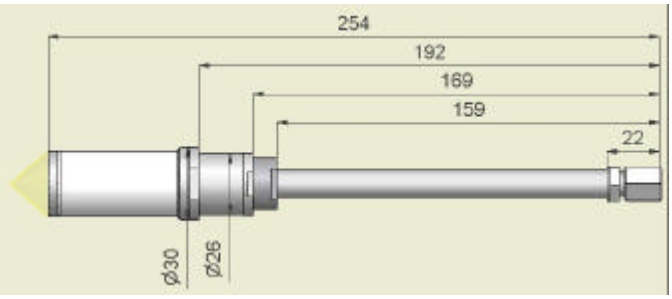

Fig. 4.18: Dimensions of a pore water pressure sensor

The new pressure sensor has the advantage that the required membrane thickness is much easier to fabricate compared to previous design resulting in a very easy change of pressure ranges.

The maximum range of the pore water pressure sensor depends on the thickness of the membrane. For each thickness of a membrane there is a pressure where the material undergoes a deformation. This is the maximum pressure that might be applied to the sensor in order not to damage the sensor. The thickness of the membrane has to be chosen in order to fit the expected measurement range.

In order to satisfy the high temperature conditions two problems needed to be solved. The first problem was to fix the fiber into the capillaries. The standard glue didn't resist the high temperature and created a lot of pre-strain losses. The solution is a new type of glue: EPO-TEK 353ND. This is a heat curing epoxy, designed for high temperature applications. This glue works properly at 200°C but it will also endure temperatures in the 300-400°C range for several minutes.

The second problem arises by using standard o-seals. These could only withstand a temperature of 90°C. At higher temperature the o-seal will melt yielding a leakage from the outside of the sensor to the inside. This will damage the fiber and influence the measured results. Another kind of o-seals gave the solution for this problem. It was the 'Viton' o-seal that can resist a temperature of 200°C.

Fig. 4.19:

Three versions of a porewater pressure sensor

The final porewater pressure sensor is available in three different versions as shown in Fig. 4.19. The first version is the thread version. The porewater pressure sensor can be foreseen of a customized thread such that the sensor can be screwed on for example a pipeline. The second version is foreseen of a cylindrical porous stone and may be used for embedding the sensor into all types of ground layers. The third version is with a flat porous stone. This type is used to measure liquid pressures in for example liquid tanks.

4.5.2. Calibration method

The calibration method has also been further developed. In the past, the pressure sensors were calibrated by recording the wavelength difference between the temperature and strain FBG as function of pressure. The wavelength difference was taken in order to compensate for the intrinsic temperature sensitivity of the gratings. However, this method does not take into account the effect of the thermal expansion of the housing on the strain FBG.

The wavelength of the strain FBG has been recorded for a stainless steel pressure cell at different temperatures but each time for atmospheric pressure. This results in a wavelength difference that is not constant at all. This can be explained by the thermal expansion of the inner tube in the housing that is causing a strain on the strain FBG when temperature increases, resulting into an extra wavelength increase.

In order to take these effects into account, a new calibration method has been used based on a more detailed study of the behavior of the pressure sensors for different temperatures. The final equation of the pressure can be written as:

$$P = A + B \cdot l_T + C \cdot l_T^2 - D \cdot \Delta l \qquad (4.8)$$

with A, B, C and D constants, λ_T wavelength of temperature grating.

The same calibration method can also be used for the new titanium porewater pressure cells. The temperature dependence is smaller than with the stainless steel sensor due to the lower expansion coefficient of the titanium material.

4.6. Total pressure sensor

A new design for a total pressure sensor has been developed. The sensor is designed for measuring pressures up to 150 bar at temperatures up to 180°C. In general, the total pressure sensor cell has the same design as the porewater pressure sensor. The only difference is the connection of the membrane with an oil filled pressure plate that is transferring the load on the pressure plate to the membrane. So each porewater pressure sensor has the capability to be transformed to a total pressure sensor.

A new element on this sensor is the design of the oil filled pressure plate, and how to fill it with hydraulic oil.

4.6.1. Sensor design

Fig. 4.20 shows the dimensions of the total pressure sensor that has the same design as the porewater pressure sensor. The oil filled pressure plate is just an extra component.

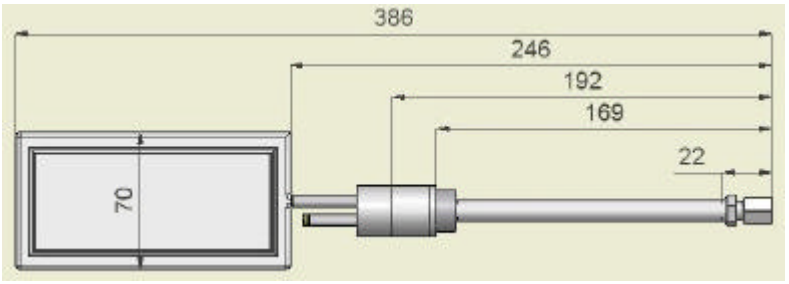

Fig. 4.20:

Dimensions of a total pressure sensor

The pressure plate exists of 2 stainless steel or titanium plates that are welded to each other. A little gap between the two plates need to be foreseen. This gap will be filled with hydraulic

oil which is used to transmit the pressure on the pressure plate to the surface of the membrane. Fig. 4.21 shows a photo of a pressure plate. When filling the pressure plate with oil, it is very important that there are no air-bubbles in the plate. An air-bubble will cause a perforation of the oil pad at high pressures. This will damage the oil pad and the measurements.

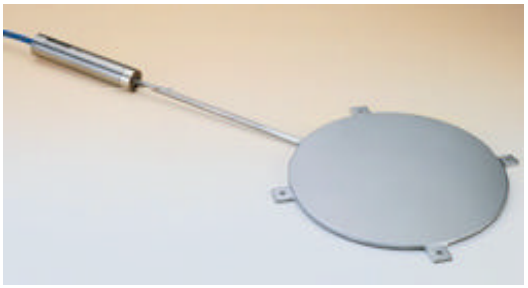

Fig. 4.21: Photo of a pressure plate

In order to obtain this, a special set-up and procedure has been used that takes more or less 4 hours to fill the oil pad correctly. At the end of this process, an internal pressure of +/- 1.4 bar will be maintained. This will guarantee the well functioning of the oil pad. The calibration method is the same as for the porewater pressure sensor.

4.7. Series configuration design for pressure sensors

The problem with the normal pressure cell design is that the fiber can not pass trough the sensor due to the presence of the membrane. The fiber enters the pressure sensor at one side and is stopped just before the membrane. The only way to obtain a series configuration is turning the fiber over 180° such that the fiber can leave the sensor along the same way as it enters the sensor. This design is shown in Fig. 4.22. There is one major problem with this solution. Due to the strong bend that the fiber needs to make (radius 8 mm) the losses of the standard SMF28 fibers become too much such that no signal can be detected anymore. The maximum bend radius of a standard SMF28 fiber is around 2 cm which is much higher than the available bend radius.

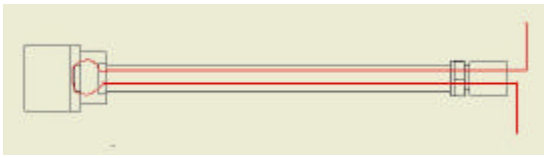

Fig. 4.22:
Fibre path for establishing series configuration.

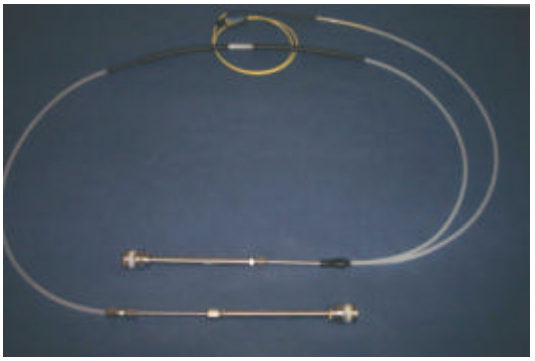

Fig. 4.23:
Serial configuration of two porewater pressure sensors

In order to solve this problem, tests have been performed using a special fiber from Stocker Yale: BIF-1550-L2. This fiber is a bend insensitive fiber (< 0.01 dB loss for 30 loops with 6 mm radius). A serial configuration has been developed using this fiber after splicing the fiber to a standard fiber containing the gratings. Figure 4.23 shows a photo of the serial configuration. No significant losses have been observed with this set-up and a proper functioning of the sensors could be established.

An in-situ test of porewater pressure and total pressure sensors has been started at the Äspö Underground Research Laboratory in Sweden. The sensors have been installed in “Temperature Buffer Test” (TBT) [30].

Due to the high corrosive and high temperature environment the sensors have been fabricated with titanium as housing and membrane material. The test period will be 5 to 10 years and the results of the long-term test will be reported in the research project named “MUSTER”.

Technical data of the currently available sensors are listed in table 4.2 and 4.3.

Type	Range	Resolution	Accuracy		Hysteresis
			Typical	Maximum	
WP-FOSS 5	5 bar	0.01 bar	0.05 bar	0.1 bar	< 1%
WP-FOSS 10	10 bar	0.01 bar	0.05 bar	0.1 bar	< 1%
WP-FOSS 50	50 bar	0.075 bar	0.35 bar	0.75 bar	< 0.5%

Tab 4.2: Specifications of the pore water pressure sensor

Type	Range	Resolution	Accuracy		Hysteresis
			Typical	Maximum	
M-TP-FOS10	10 bar	0.01 bar	0.05 bar	0.1 bar	< 1% F.S.
M-TP-FOS50	50 bar	0.05 bar	0.25 bar	0.55 bar	< 0.5% F.S.
M-TP-FOS150	150 bar	0.075 bar	0.35 bar	0.75 bar	< 0.5% F.S.
M-TP-FOS400	400 bar	0.075 bar	0.35 bar	0.75 bar	< 0.5% F.S.

Tab. 4.3: Specifications of the total pressure sensor

The titanium based sensors are designed and calibrated to work in an temperature environment of up to 180 °C.

4.8. Humidity sensor

4.8.1. State at the beginning of the project

The design of the hydrogel sensor is shown in Figure 4.24. The sensor consists of a stainless steel tube, which has at one end a hydrogel film. At each end side of the tube, a mechanism is foreseen to fix a capillary. Between both capillaries a FBG is stretched. When the hydrogel film comes into contact with high humidity levels, the film will swell and an elongation of the fiber occurs. This results in an increase of the strain on the FBG, what results into a wavelength shift:

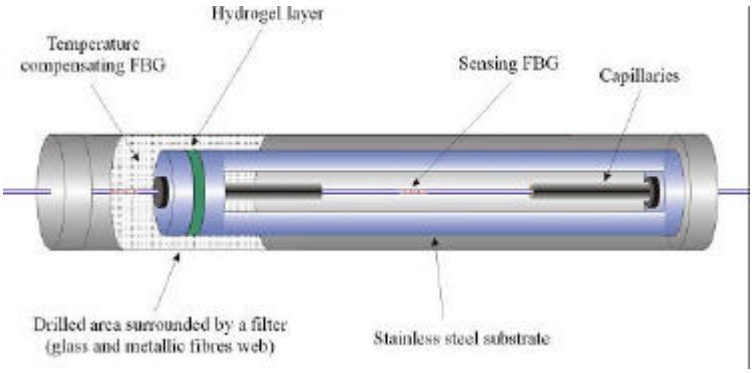

Fig. 4.24: Design of humidity sensor

The temperature effects of the strained grating are compensated using a second FBG which remains in an unstressed condition. However, this compensation does only take into account the intrinsic temperature sensitivity of the FBG but does not take into account the effect of the thermal expansion of the sensor housing.

During the project, the hydrogel has further been characterized. The complete temperature behavior has been analyzed. A new interpretation method is proposed that does take into account the thermal expansion of the housing. Furthermore, the influence of pH levels, salt solutions and radioactive radiation has been analyzed.

4.8.2. Total temperature compensation

So far, no thermal expansion effect had been taken into account when looking to the response of the different wavelengths. Nevertheless, a significant influence can be expected. Therefore, a new calibration method needs to be used that does take into account this thermal expansion. The method will be indicated by 'Total Temperature Compensation'. Figure 4.25 shows the schematic representation of the thermal expansion of the housing. Due to the increasing temperature, the capillaries as well as the inner stainless steel tube will elongate resulting in a net elongation of the stressed fiber of:

$$\Delta L = \Delta L_1 - \Delta L_2 - \Delta L_3 = L_1 \cdot \alpha_{SS} - (L_2 + L_3) \cdot \alpha_{cap} \qquad (4.9)$$

with ΔL_1 the elongation of the inner tube between the two capillary fixation points, ΔL_2 and ΔL_3 the elongation of the capillaries starting from the fixation point, α_{ss} and α_{cap} the thermal expansion coefficients of the inner tube and the capillaries. Using equation 4.9 a good correspondence with the experimental sensor response has been obtained.

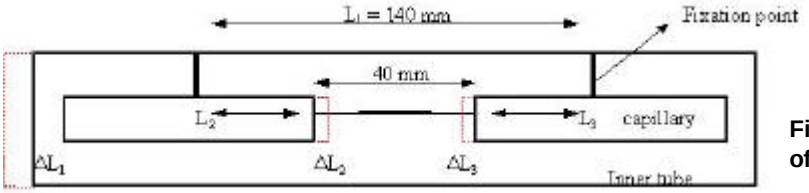

Fig. 4.25: Schematic representation of thermal expansion.

As a conclusion the influence of the thermal expansion of the housing does induce an effect on the response of the hydrogel sensor that can not be neglected. In future, the temperature sensitivity of the temperature FBG (S_T) and the stressed FBG (S_S) will be measured at low humidity level (ex. 50%). The total temperature compensated sensor response can then be given by:

$$response = \Delta(l_S - \frac{S_S}{S_T} \cdot l_T) \qquad (4.10)$$

With λ_S the wavelength of the stressed FBG
λ_T the wavelength of the temperature compensating FBG

This response does take into account the thermal expansion of the housing and will only be influenced by changes in humidity level.

4.8.3. Influence of pH-level

The influence of the pH-level of the fluid that comes into contact with the hydrogel film has been investigated. Two pH levels have been tested: pH 2 and pH 8. Fig. 4.26 shows the sensor responses for pH 2 and pH 8 solution. The sensors have been put into the solution for 1 day and drying during another 3 days afterwards. It has been observed that both responses show a similar behavior. The sensors also show a hysteresis effect after drying but this is also present for normal pH levels. It can therefore be concluded that the humidity sensor is reacting very well at different pH levels.

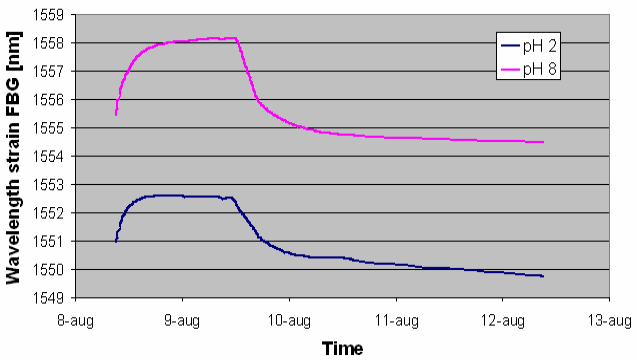

Fig. 4.26:
Influence of pH level on humidity sensor response

4.8.4. Response in salt water environment

With regard to an application at the Morsleben site located in salt host rock the response of the hydrogel sensor in a salt environment has been investigated. A hydrogel sensor containing 3 hydrogel films had been fabricated. The sensor was put into a salt solution coming from the Morsleben site resulting in a good sensor response. An increase in wavelength difference from 2.2 to 4 nm has been observed. Nevertheless, the sensor does show a higher hysteresis for the salt solution than for normal water. This can possibly be attributed to a crystallization of the salt in the hydrogel films, causing strain on the FBG.

4.8.5. Influence of radioactive radiation

With regard to an application in a radioactive environment the influence of radioactive radiation on the hydrogel film has been analyzed. Two hydrogel films where radiated with γ-radiation: the first sensor with a dose of 100 GY and the second with a dose of 1 KGY. After the radiation, the sensor was mounted into a hydrogel sensor and analyzed into a climatic chamber. The humidity was initially set at 50%. After stabilizing, the humidity level was increased with a slope 0.02%/min up to a final level of 95%. This value was fixed for one day after which the initial value of 50% was reset. The result is that both sensors start reacting at a humidity level around 80%.

Furthermore, the signal stabilizes very slowly at a humidity level of 95% and a hysteresis effect can be observed when going back to the initial humidity value of 50%. This behavior is quite similar as with the non-radiated hydrogel films. It can therefore be concluded that the radiation with a dose lower or equal to 1 KGY does not show a significant effect on the response of the hydrogel film.

4.8.6. Field tests

In-situ tests of the sensor have been performed at the Grimsel Test Site (GTS) in Switzerland and at the Morsleben site. In the framework of a gas injection test at the GTS, sensors have been embedded in barrier material consisting of sand and bentonite. Besides the loss of a few sensors right after sealing of the experiment, it came out during the experiment that there is a significant dependence on the pressure of the fluid in a way not being expected. Figure 4.27 shows the sensor response together with the fluid pressure development. Of course the sensor shows a significant indication of fluid arrival as marked with an arrow, but a further interpretation of the increase of fluid amount within the barrier material is not possible, since the later signals are overlapped by the pressure dependence indicated by a decrease of the response.

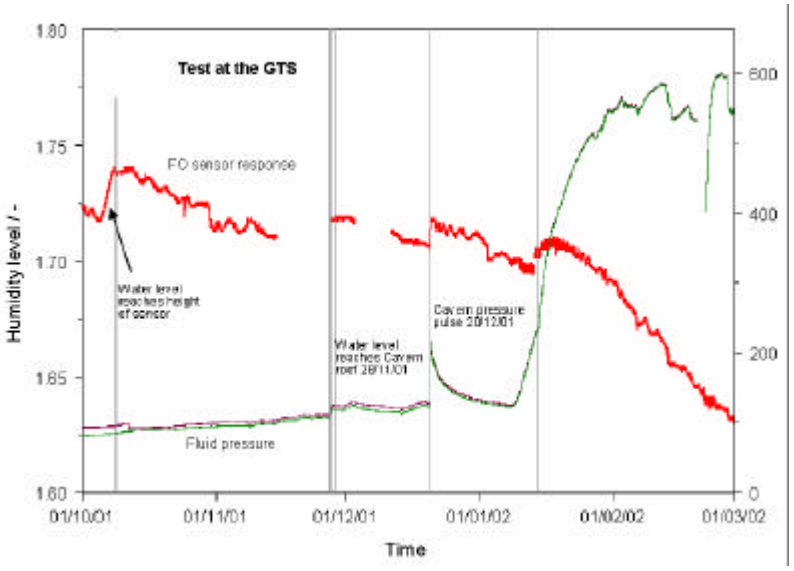

Fig. 4.27: Extraction of test measurement results at the GTS

Another test has been performed at the Morsleben site in a salt environment. In this test the sensor has been installed at the roof of an underground opening to monitor fluid inflow or "dropping rates" respectively at selective locations. A photo of the installed sensor is shown on figure 4.28 and measurement results are shown on figure 4.29.

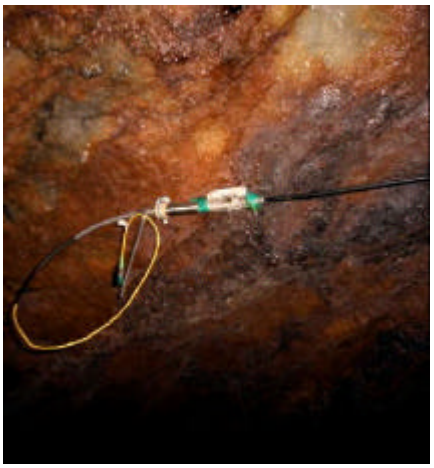

Fig. 4.28:
Photo of sensor installation at a cavity roof at the Morsleben site

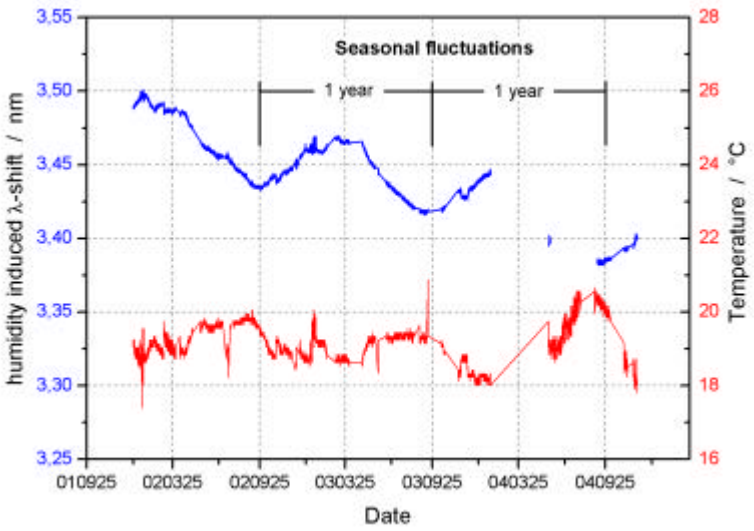

Fig. 4.29:
Test measurement results (humidity and temperature) at the Morsleben site

As can be seen, the brine inflow is not constant but varies periodically. Looking at the time scale this can be attributed to seasonal fluctuations over periods of 1 year. In addition, the measurement results of the temperature FBG at the sensor is plotted in figure 4.28 to check for any temperature dependence. A more or less constant temperature has been observed and compensated as described in chapter 4.8.2. Thus, the fluctuation can be stated to be just humidity dependent.

4.9. Hydrogen sensor

4.9.1. Basics

The metal-hydrogen system consists of a metallic material, hydrogen gas, and an interface region between them (see Fig. 4.30).

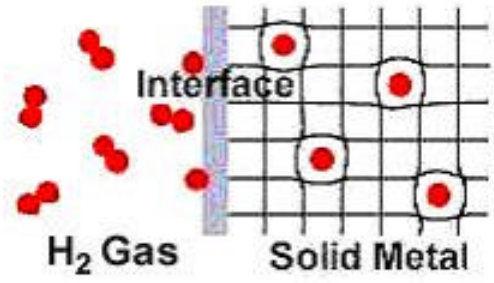

Fig. 4.30: Simplified Model of Metal-Hydrogen Interaction

Hydrogen gas adsorbs onto the interface region. At the interface, the molecule is dissociated into individual hydrogen atoms that are able to absorb or dissolve into the metal phase. The random dissolution of hydrogen atoms in the metal phase is known as the α-phase. Within the metallic phase, the hydrogen atoms can start to arrange themselves in a specific configuration with the metal atoms, forming the metal hydride phase, called the β-phase. Where and how the β-phase is nucleated and grows is a characteristic of the material.

The reaction of hydrogen with a metal can be written as a chemical reaction:

$$M + x/2\ H2 \longleftrightarrow MHx + Heat \qquad (4.11)$$

The double arrow indicates that the reaction is reversible and exists as an equilibrium state. In other words, by changing conditions, the reaction can be made to go in either the forward or reverse direction. The heat on the right-hand side indicates that heat or energy is released when the metal hydride is formed, and thus, heat must be put in to release hydrogen from the metal hydride phase. The heat is the enthalpy (heat of formation) of the reaction and is an indication of the strength of the metal-hydrogen bond in the metal hydride phase. The equilibrium between hydrogen and metals is best described by a "Pressure–Composition" Isotherm plot, called a "PCT" curve [22]. Idealized PCT curves are shown in Fig. 4.31.

The sloping part on the left side of the PCT curves shows that - in case of only the α-phase is present - large changes in hydrogen pressure yield only slightly changes of the concentration of dissolved hydrogen within the metal matrix. However, once nucleation of the β-phase starts and both the α and β-phases exist simultaneously, a large increase in the hydrogen concentration within the metal matrix occurs over a very small change in hydrogen pressure. Once the material has become saturated with the β-phase, again only slight hydrogen uptake occurs with large changes in hydrogen pressure. The flat region, which is characteristic of the coexistence of two phases in equilibrium, is called the equilibrium plateau pressure and is a characteristic of the material. Also note that at higher temperatures, it takes higher hydrogen pressures to cause the large uptake of hydrogen gas [23].

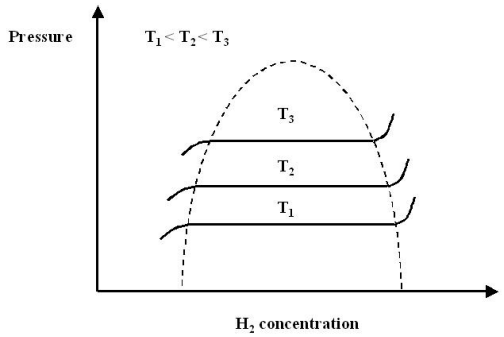

Fig. 4.31: Idealised PCT curves for 3 temperatures

The palladium-hydrogen system has the property that at normal temperature, palladium can absorb up to 900 times its own volume of hydrogen. This absorption is accompanied by extensive plastic deformation of the metal, but without mechanical or chemical disintegration. A couple of investigations [14],...,[20] have been performed showing a sensor response depending on the presence of CO. As an example the hydrogen response of a Pd based hydrogen sensor with and without the presence of CO is shown in Figure 4.31 [13]. Adsorption as well as the desorption response is much slower in the presence of CO. In order to investigate this in detail a new term is introduced: the impeding factor. This factor is the ratio of the slope of the response without the presence of CO on the slope of the response with the presence of CO. The impeding factor is by definition equal to 1 at zero CO coverage and is experimentally defined for different CO coverage's. This result is shown in the insert of Figure 4.32. The impeding factor is very small below CO coverage's of 0.2, while it increases exponentially above this coverage. This strong increase can not be explained by site blocking by the CO molecules but is due to an increase of the activation energy for hydrogen dissociation and hydrogen desorption with increasing CO coverage [24]...[26].

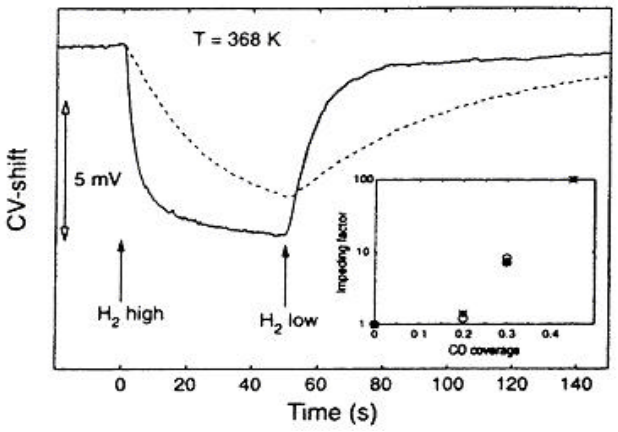

Fig. 4.32: Sensor response at 368K for a hydrogen pressure pulse between t=0 and t=50 s, in the absence (full line) and presence (dashed line) of CO. The insert shows the impeding factor as a function of CO coverage for hydrogen adsorption (*) and desorption (o) [13].

4.9.2. Hydrogen sensor design

Two sensor designs have been developed and tested indicated as sensor type I and sensor type II.

The design of sensor type I is shown in Figure 4.33. The sensor consists of a stainless steel tube, which has a palladium disc at one end and a capillary at each end side of the tube. Between both capillaries a FBG is stretched. When the palladium disc absorbs hydrogen, the disc will swell and an elongation of the tube occurs. This results in an increase of the strain on the FBG, which gives at his turn a wavelength shift of:

$$\Delta\lambda = 1.2 \cdot 10^6 \cdot \varepsilon_P(P_{H2})\ th_{Palladium} / L_{FBG} \qquad (4.12)$$

With $\Delta\lambda$ the wavelength shift in pm; $\varepsilon_P(P_{H2})$, the strain on the palladium material caused by the hydrogen pressure P_{H2}; $th_{Palladium}$, the thickness of the palladium disc; L_{FBG} , the length of the fiber hosting the stretched FBG.

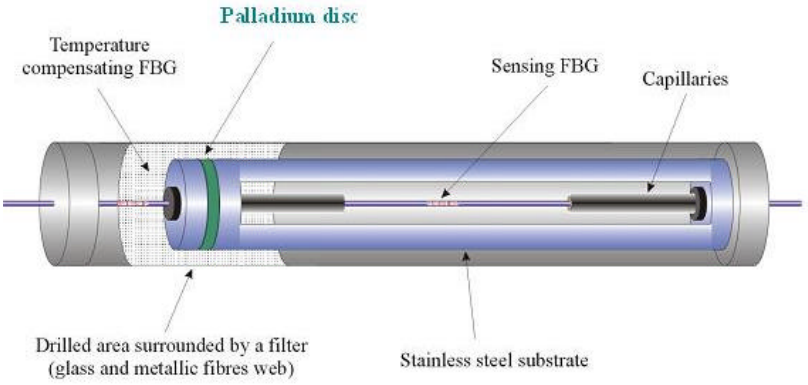

Fig. 4.33:

Design of hydrogen sensor I

The sensitivity and dynamic range of the hydrogen sensor can be applied by choosing the thickness of the palladium disc or the length of the stretched FBG. The palladium disc has a thickness of 0.5 mm and the length of the fiber hosting the FBG is equal to 45 mm. As a consequence, the wavelength shift due to hydrogen presence is given by:

$$\Delta\lambda = 1.2 \cdot 10^6 \cdot \varepsilon_P(P_{H2}) \cdot (1/90) \qquad (4.13)$$

It needs also to be mentioned that temperature effects on the grating are compensated by using a second FBG which remains in an unstressed condition. However, this compensation does not take into account the effect of the sensor housing since the distance between both capillaries is also influenced by the thermal expansion coefficient of this housing. Therefore, a similar compensation method as with the humidity sensor was applied.

The design of sensor II is based on the concept of the temperature sensor. Figure 4.34 shows the design of the sensor. The sensor exists of 3 capillaries that are made of stainless steel and are used to fix the fiber by gluing. These capillaries have an outward diameter of 2 mm at one end and an outward diameter of 1.5 mm at the other end. This allows to put these capillaries into the larger Pd capillary which has a purity of 99.95%, an outward diameter of 2 mm and an inner diameter of 1.6 mm. Figure 4.35 shows a photo of the sensor. When the Pd capillary absorbs hydrogen, the capillary will expand resulting in a strain on the fiber.

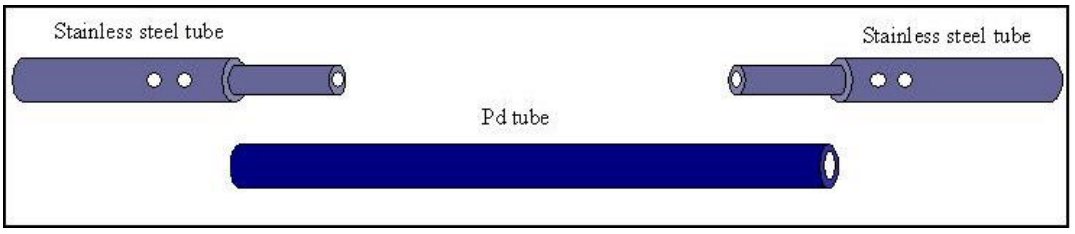

Fig. 4.34: Design of hydrogen sensor II

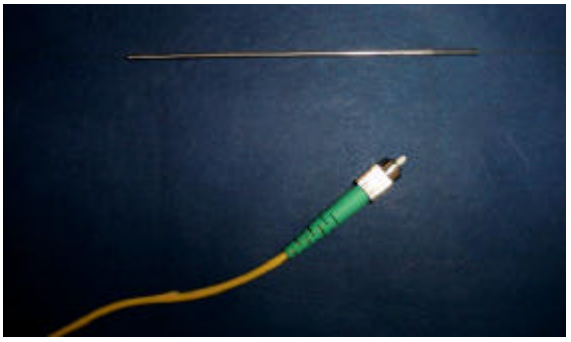

Fig. 4.35: Photo of the hydrogen sensor II

The wavelength shift of the grating due to the presence of hydrogen is given by:

$$\Delta\lambda = 1.2 \cdot 10^{6} \cdot \varepsilon_P(P_{H2})\, L_{Pall} / L_{FBG} \qquad (4.14)$$

With $\Delta\lambda$ the wavelength shift in [pm]; $\varepsilon_P(P_{H2})$, the strain on the palladium material caused by the hydrogen pressure P_{H2}; $L_{Palladium}$, the length of the palladium tube; L_{FBG}, the length of the fiber hosting the stretched FBG. This length is equal to the distance between the fixation points on the two stainless steel capillaries. As a consequence, by changing the position of these fixation points, the sensitivity can be changed.

For the test design L_{pall} was chosen to be equal to L_{FBG}. As a consequence, the wavelength shift is given by:

$$\Delta\lambda = 1.2 \cdot 10^{6} \cdot \varepsilon_P(P_{H2}) \qquad (4.15)$$

Compared with sensor type I, sensor type II was expected to be 90 times more sensitive. Furthermore, a separate FBG has been used during the experiments for temperature compensation of the FBG wavelength. Additionally, the influence of the thermal expansion of the sensor should be taken into account in future. However, for the experiments discussed in this report, the temperature compensation is not that important to interpret the behavior of the sensor since the temperature is kept more or less stable during the experiments.

4.9.3. Calibration set-up

The calibration system consists of a vacuum chamber, which is equipped with a rotary pump and a turbo pump. The base pressure of the vacuum system is equal to 10^{-6} mbar. In order to bring hydrogen into the vacuum chamber, forming gas with a composition of 10% H_2 and 90% N_2 was used. The calibration was performed by measuring the wavelength change in function of the partial hydrogen pressure. The temperature was kept stable at 23°C during the experiments. Finally, in order to measure the hydrogen sensors, a special flange with a fiber throughput was developed.

In a later phase of the project the calibration system has been changed now consisting of a chamber that can be filled with forming gas. This is a mixture of H_2 in N_2. A calibration can be performed by using different mixtures of forming gas or by changing the pressure in the chamber. The pressure can be changed between 1 and 8 bar. This allows to change the partial pressure of the hydrogen concentration using one mixture. For safety reasons, the hydrogen concentration never exceeded 4.2% H_2.

4.9.4. Experimental results

Sensor type I: The wavelength of sensor I was measured for partial hydrogen pressures ranging between 0 and 100 mbar. Unfortunately, this sensor was not able to detect a response under the given experimental conditions. A possible explanation for this might be that the contact surface of the Pd-disc with the hydrogen molecules is much to small. The design of sensor I had therefore been modified in order to increase this contact surface.

Sensor type II: The wavelength of sensor II was measured for partial hydrogen pressures ranging between 0 and 50 mbar. In Figure 4.36 the wavelength response is shown in function of the partial pressure. The vertical lines in the plot are caused by a slow absorption process of the hydrogen by the Pd (When the hydrogen pressure is increased, the wave-

length increases very slowly). It can be observed that a strong response is becoming visible starting from hydrogen pressures around 18 mbar. This strong response can be explained by the formation of the β-phase at this pressure. This is also in good agreement with the results of Bévenot et al. [21] who observed that the β-phase is formed between the 15 and 20 mbar. By further increasing the hydrogen pressure up to 50 mbar, a wavelength shift of 180 pm could be observed. The problem is, that the time period to reach full saturation of the palladium is still rather long (see A, B, C).

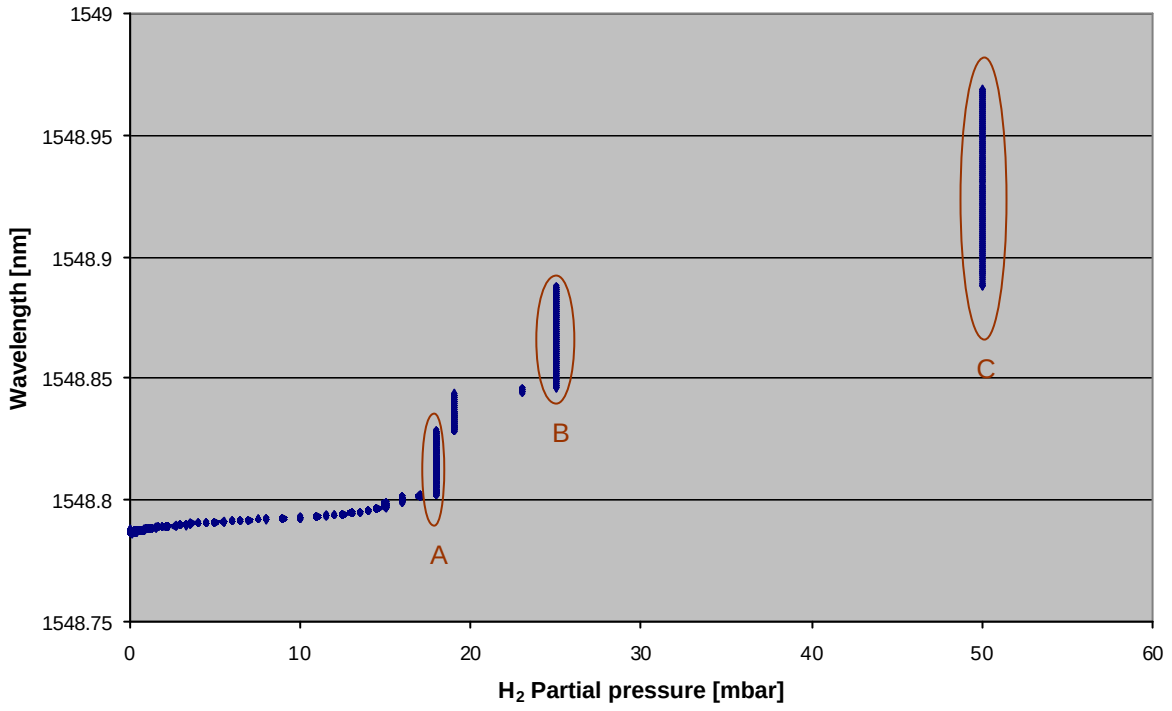

Fig. 4.36: Response of sensor II

Thus, at the time being, the current design of the sensor works well as an indicator in case of hydrogen appearance. Due to the long time for reaching full saturation a calibration to quantify the H_2 contents is difficult. The main problem is the small surface/volume ratio of the Pd material. In order to enhance the time to reach saturation a new design of the sensor lay-out has been developed with a small surface volume ratio. The sensor consists of a naked FBG that directly has been coated using Pd. Due to the presence of hydrogen, the Pd will swell and induce a strain on the FBG, resulting into a wavelength shift.

So far, a lot of effort has been spent for manufacturing of this design type. The Pd is deposited using a plating technology. But unfortunately, some problems still remain concerning a reliable fixation of the coating. In order to solve these problems an intermediate layer between the glass fiber and the Pd coating that acts as a buffer between the glass and the Pd seems to be a promising solution. It is for example known that when a thin Ti layer as intermediate layer is used, a good adhesion can be achieved [15].

4.10. pH sensor

4.10.1. Working principle

The pH probe consists of two bundled optical fibers facing a reflector (Figure 4.37). A dye is coated onto the reflector. The input fiber couples light from the opto-electronic unit into the

gap between the fiber tips and the reflector. Light propagates through the dye, is reflected, and then re-coupled into the output fiber. The opto-electronic unit measures the reflected light's intensity [27], [28].

The dye's optical absorption depends upon the pH of the solution surrounding the probe. Thus, the ratio between the emitted optical power and the detected optical power provides a measure of the pH-value

As a simple means to compensate for extrinsic losses due to, for example turbidity effects, a reference channel is included in the probe, and only half of the reflector surface is coated with the dye. The reference channel is identical to the signal channel, but the reference channel fibers face the uncoated part of the reflector. As a consequence, the difference between the signal absorption and the reference absorption of the reference channel corresponds to the extrinsic optical losses, that can thus be compensated.

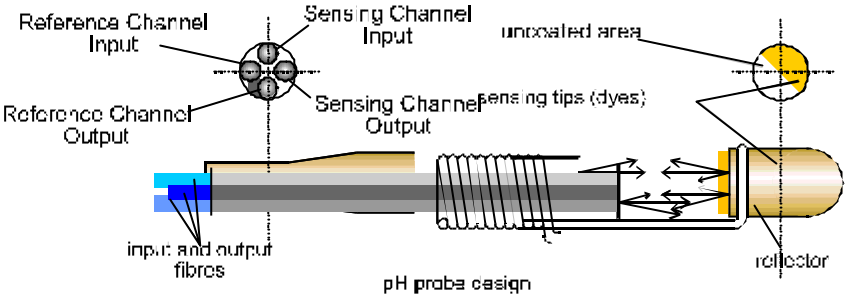

Fig. 4.37: Principle design of pH sensor

4.10.2. Measurement principle of the opto-electronic unit

The current pH system consists of a probe containing methyl red. Methyl red has the properties that the reflection of light is dependent on wavelength but also on the pH level of the contacting fluid. As a consequence, by measuring the reflection characteristics of the methyl red as function of the wavelength, the pH value can be determined.

Fig. 4.38: Opto-electronic unit

Figure 4.38 shows the opto-electronic unit that has been developed. The system is based on the utilization of only one LED, which is modulated in order to allow a referenced measurement.

The modulation is carried out by driving the LED in two different states with two different currents. By changing the driving current the emission of the LED changes: the change is roughly 10 nm. The difference between the detected signals in correspondence to the emission at these two different wavelengths gives the possibility of measuring the slope of the absorption spectrum which is dependent on the pH level. The method is more sensitive at the wavelength at which the absorption curve has a higher slope. In the case of methyl red the wavelength is around 505 nm.

Therefore, with this method the slope of the absorption curve is measured: clearly there is a different slope for each pH value. The important aspect is that any interferences and fluctuations, which do not modify the slope of the absorption spectrum, do not give rise to changes in the detected signal. Hence, bending of the fiber, fluctuations of the source, turbidity (if it

introduces a constant contribution at the wavelengths of interests) do not interfere with the measurement.

Test have been carried out in order to see if there is a drift due to the photo decomposition of the immobilized dye. A test has been carried out for ten days and the result is shown in Figure 4.39. The ambient temperature has also been measured.

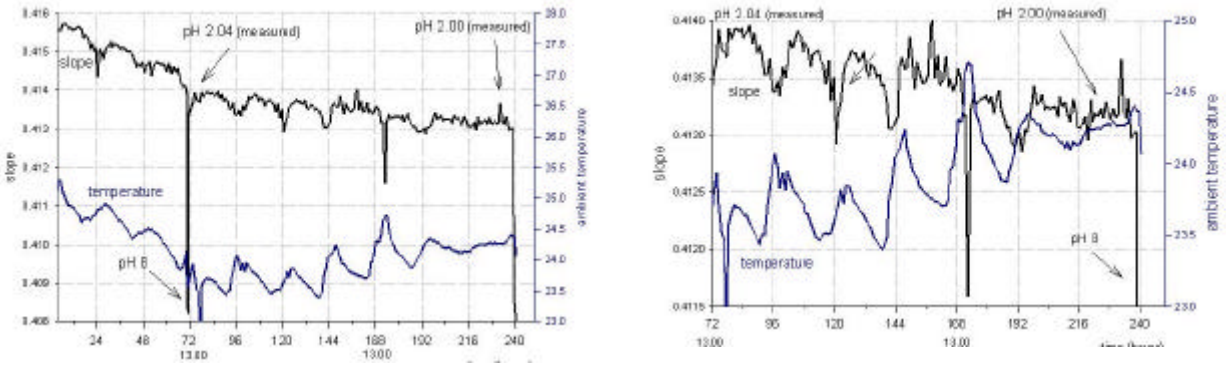

Fig. 4.39: Drift and temperature dependence of the probe characterized with the new opto-electronic unit

Methyl red, the dye immobilized on the CPGs, is characterized by a negative coefficient $\Delta(\text{slope})/\Delta T$ where T is the temperature: the detected slope at a definite pH value increases if the temperature decreases. In the first 72 hours, the drift is apparent: the temperature decreases and also the detected slope decreases, although the probe is always dipped at pH 2.04. After the hour 72, the optical power is decreased of a factor 5 and the decrease in the slope is considerably smaller; moreover, in this period the temperature increases and the decrease of the detected values of the slope is perfectly in agreement with the increase of temperature; this means that by using low optical power from hour 72 to hour 240 (six days) the drift is negligible.

This measurement also shows a non negligible dependence of the probe response to temperature. Every increase of the ambient temperature corresponds to a decrease in the detected signal. An accurate temperature characterization has therefore been carried out, by dipping the probe in buffer solutions kept at constant temperature and calibration curves have been obtained. Figure 4.40 shows the detailed measurements at a temperature of 20°C. It is noteworthy to observe that the hysteresis is negligible. The error on the detected slope based on the standard deviation of the last five detected values is $\leq 10^{-4}$. An automatic temperature compensation of the pH value has been implemented.

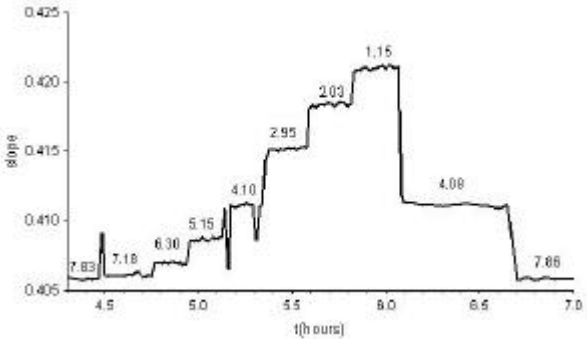

Fig. 4.40: Detail of the temperature characterization at T= 20°C

The resolution in terms of pH has been determined to be around 0.03 pH units for pH below 5. The accuracy decreases with the increasing pH; it can be considered roughly 0.08 pH units between 5 and 7. Making use of the new calibration the stability has been checked for 24 hours and no drift has been observed. The current test probe and the connection with the fibers between the opto-electronic unit and the reflectors is shown in Figure 4.41.

Fig. 4.41: Picture of the optical fibre pH test probe.

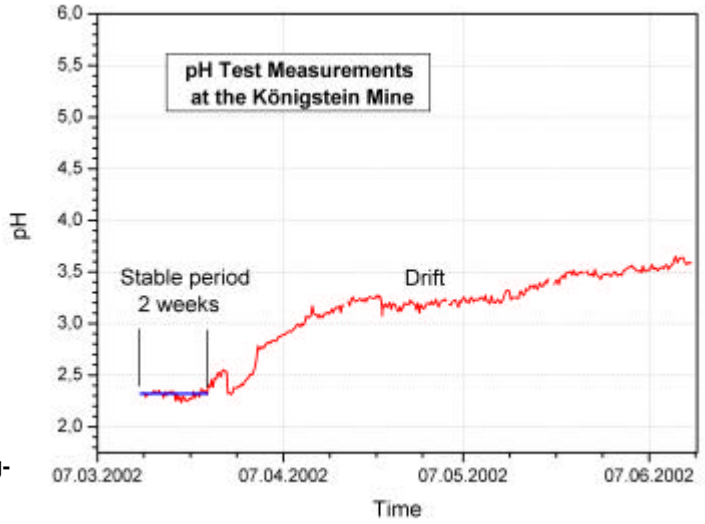

Fig. 4.42: pH-field measurements at the Königstein mine

After having achieved successful laboratory results the new probe has been tested in-situ at the Königstein mine for monitoring purposes. Figure 4.42 shows main results of the test. It has been observed that there is a maximum period of about 2 weeks in which stable results could be obtained. Any longer continuous running of the probe yield a drift of the measurement results.

At the time being two main reasons can be given for the drift.

First of all, the drift can be caused by a kind of photo-bleaching effect of the reflector's dye (photo-decomposition). After dismantling of the sensor the dye has been analyzed in the laboratory. It has been observed that the color of the used reflector was more faded what testifies a partial bleaching of the dye due to the illumination period. The second possible reason for the drift is a degeneration of the LED. The modulation of the wavelength is carried out by driving the LED in two different states with two different currents as mentioned above. For a reliable result it seems to be important that the relative change in emission power as well as the wavelength change of 10 nm is constant as function of time. If not, a drift can occur.

At the time being the technical specification of the sensor can be summarized as shown on table 4.5.

Dye	Methyl-red
Dynamic range	2-7 pH
Resolution	0.03 pH
Hysteresis	< 0.03 pH
Recalibration period	2 weeks maximum
Response time	< 1 min.

Tab. 4.4: Technical data of the current pH-sensor

The technical specifications are very good for normal short term applications compared to conventional sensors. For the purpose of long term monitoring some more research is necessary to improve the existing sensor by eliminating the drift or to use new design specifications as outlined in chapter 8.

5. Multiplexing techniques and interrogation units

5.1. Interrogation system

In the past, FBG-based sensors have been interrogated with a broadband optical source (40 nm wide) and the spectral responses of the different sensors in the network are demodulated with a standard Fabry Pérot (SFP) filter. The instrument has been named as FMUB-SFP. The SFP demodulator has been delivered on a board together with the driving/interface electronics, temperature stabilization, opto-electronics and driving/interface software modules. The calibration has been applied on every scan using two reference gratings at the beginning and the end of the spectrum.

This system shows however some shortcomings:

1. The reference gratings are temperature sensitive. A drift of the environmental temperature of the measurement unit will as a consequence also influence the calibration process.
2. Deviations from the linear behavior of the SFP can not be corrected using only the 2 reference FBGs.
3. The SFP is rather large and composed using different mechanical components that require from time to time a realignment. These misalignment problems are time consuming and reduce the reliability of the system.

In order to improve the system, the integration of a new system has been performed. The new system is based on the FBG-IS from Micron Optics. The schematic diagram of the system is shown in Figure 5.1. The major difference is the type of filter device and type of reference device.

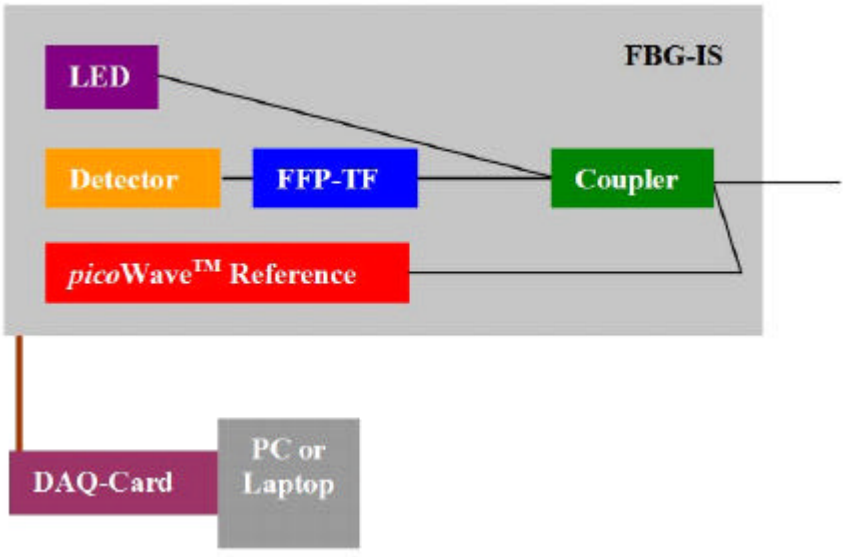

Fig. 5.1: Schematic lay-out of the FBG-IS

The filter device is a Fiber Fabry Perot Tunable filter (FFP-TF) which is shown in Figure 5.2. The FFP-TF is an optical cavity composed within an optical fiber which is used to scan the wavelength range. No lenses, no collimating optics, just simply fiber and mirrors.

This true fiber cavity constitutes FFP Technology. All the high optical resolution advantage of the "old", bulk optic device is preserved, but with three critical distinctions:

- FFP Technology has optical fiber inside the etalon which guides the light with each bounce between the mirrors. The extreme alignment, temperature, and vibration sensitivities of the "old", bulk-optic Fabry-Perot interferometers are gone. In fact, the alignment sensitivity of FFP technology is no more than that of an individual single-mode optical fiber splice or connector.
- FFP Technology has natural fiber connection compatibility unlike lenses or integrated wave guides, which encounter fundamental connection difficulties.
- FFP Technology is combined with the highest resolution mechanical positioning devices, Piezoelectric Transducers (PZTs), to position the mirrors in FFPs. PZTs are used in atomic force microscopes to position elements to sub-atomic dimensions. This level of mechanical resolution ensures stable, smooth, repeatable tuning of any FFP filter.

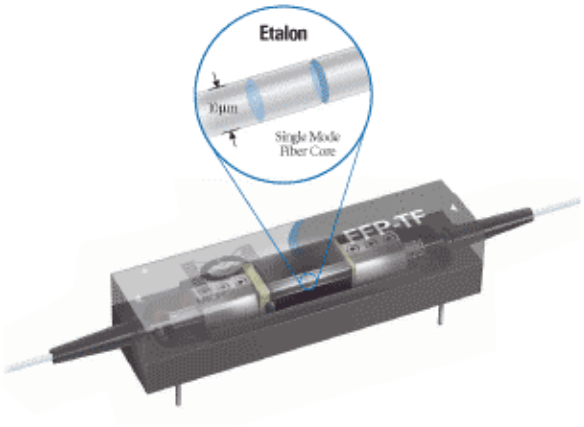

Fig. 5.2: Schematic design of FFP-TF

These three critical innovations allow the FFPs optical response to truly follow the Airy function from the top of its low-loss peak down to the very bottom of its stop band, and to be smoothly and precisely controlled over all points in between. Furthermore, the FBG-IS makes use of the picoWave reference module. This is a Fiber Fabry-Perot Interferometer (FFP-I), based on a fixed interferometer design with smooth, uniformly spaced transmission peaks. The FFP-I consists of a lensless plane Fabry-Perot interferometer with a single-mode optical fiber wave guide between two highly reflective multilayer mirrors. The FFP-I is manufactured with fiber pigtails so no alignment or mode-matching is required. The distances between peaks (FSR) may be fit exactly to customer specifications and a TEC package is available for thermal stability and minor adjustments of the bandpass frequency or wavelength.

The picoWave gives a multi-wavelength reference that enables real time wavelength calibration to picometer accuracy. Combining the uniform spacing of the FFP-I, a wavelength marker of a Fiber Bragg Grating, and a built-in TEC for thermal stability, the picoWave® makes an ideal calibrated wavelength reference over the entire scanning interval of the FBG-IS. As a consequence, a very good compensation for linearity effects can be carried out. Notice that due to the TEC, no ambient temperature influence is present here.

These both components make from the FBG-IS a high resolution and reliable system. The specifications are shown in Table 5.1.

Optical	
Number of Optical Channels	1
Maximum Number of FBG Sensors/Channel	31
Wavelength Range	1528 - 1568 nm
Calibrated Accuracy	+/- 10 pm
Repeatability	+/- 5 pm
Optical Power/Channel	-55 dBm (approximate)
Dynamic Range	12 dB
Resolution	< 1 pm
Scan Frequency	52.4 Hz
Minimum FBG Spacing	0.5 nm
Optical Connector	FC/SPC
Computer Interface Card	PC or PC Card (PCMCIA)
Operating Temperature	10° - 40° C
Dimensions	69 x 277 x 267 mm
Weight	2.7 kg

Table 5.1:
Specifications of the FBG-IS

5.2. Software

The complete software, developed for the FMU-B-SFP has been adapted for the new hardware and further extended. Three different types of software programs have been newly developed: control software, calibration software and monitoring software. All developments have been done in the LabView software environment.

Control software: The control software aims to detect the position and the amplitude of the spectral responses on an optical line along which FBGs are connected. The software displays the amplitude responses and can also measure the FBG wavelengths. Its main objective is to allow the user to control the integrity of an optical line.

Calibration software: The calibration software allows to calibrate one FBG based sensor. The software allows to visualize and measure the signal the same way as the control software. But it can perform the calibration of a complete FBG based sensor and not only of one FBG or several FBGs. If the FBG is temperature compensated, the FBG-FOS implements two FBGs. To achieve differential temperature compensation, the wavelength difference between the FBGs is be measured along with its standard deviation. To achieve total temperature compensation, each FBG wavelength is measured separately along with its own standard deviation.

Monitoring software: The monitoring software performs automatically continuous or periodical acquisition and storage of the measurements of FBG based sensors. Three main setting parts can be distinguished: system settings, sensor settings and network settings. Once everything has been initialized, the measurements sequence starts and performs continuously and/or periodically the demultiplexing of the FBG-FOSs (Wavelength Division Multiplexing) and performs continuously and/or periodically the measurements of the parameter addressed by the sensors on each optical line in the fiber optical sensing network, one line after each other.

5.3. Optical switching

At the beginning of the project efforts have been put in the design of less expensive optical switches. A type of an 1x3 optical switch by using different 1x2 optical switches in cascade has been designed. The optical switch (OS) comprises two 1x2 optical switches driven by a CMOS or TTL logic. The required electronics has been soldered to interface the 1x2 switches to the computer through a very basic digital input/output interface card.

The first 1x2-OS (OS1) connects directly line 3 to the demodulator whereas it connects line 1 and line 2 through the second (cascaded) 1x2-OS (OS2). This configuration is required since the optical loss are the larger along line 3 and the signal need to propagate through as few as possible components in order to experience as low as possible optical loss. In any case, the amplitudes of the signals are all at least twice the detection threshold which is itself about 5 times the noise level. Figure 5.3 summarizes the optical switch configuration along with its optical budget. Figure 5.4 shows some pictures of the actual developed 1x3 optical switch.

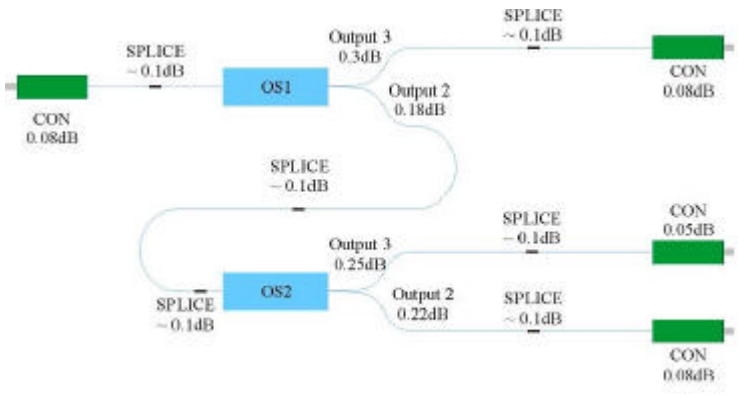

Fig. 5.3: Optical switch configuration along with its optical budget and its optical loss

The control of the switch is done using a software program developed in LabView and has been integrated into the monitoring software described above. The developed optical switch has successfully been used for the installation at the Grimsel Test Site.

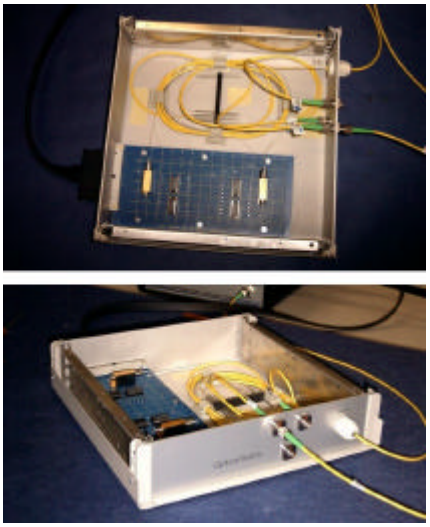

Fig. 5.4: 1x3 optical switch design.

More generally, this “shot” development was the preliminary to a larger scale development of an optical switch for the FMU-B–XXX. For switching up to 4 lines, it is interesting to cascade several 1x2 OSs to build up a 1xN OS (N = 2, 3). This is modular and cost effective. Beyond 4 lines, a 1x4 OS cascaded with 1x2 OS(s) can be used to build up a 1xM OS (M = 4,5,6,7). From 8 lines, a 1x8 OS can be cascaded with 1x2 OS etc.

This way to build up an optical switch is flexible, electrically efficient since the driving signals are most of the time of the same kind (CMOS/TTL logic) and requires only slight adaptation of the board, optically very efficient since the power budget can be optimized and economically the best way to keep the cost as low as possible.

Nevertheless, due to new developments in the telecommunication market, it did became unfavorable to built the optical switches ourselves. The costs of the optical switches has drastically be reduced during the last two years. It was therefore concluded to use commercial available OEM optical switches in stead of building own switching systems.

5.4. Evaluation of passive optical components

5.4.1. Connector evaluation

Different optical connector types have been investigated. In the past, the FC/APC connectors have been extensively used. A pending problem with the FC/APC connectors is the contamination with dust of the connectors during maintenance when the connectors are in a disconnected state. Therefore, alternatives have been searched and found: the E2000 connector.

The E2000 connector holds a single fiber in a ceramic Ferrule. E2000’s are small form factor connectors with a moulded plastic body similar to that of an LC Connector. The E2000 also exhibits a push-pull latching mechanism, and integrates a protective cap over the ferrule, which acts as a dust shield and shields users from laser emissions, see Figure 5.5. The protective cap is loaded with an integrated spring to ensure proper closing of the cap. Therefore, this type of connector is very well suited for usage in dusty environments like in mines.

Fig. 5.5: Photo E2000 connector

The first field tests with these connectors have been performed in the mine at Morsleben (Germany) and Äspö (Sweden). The experience so far is excellent. It has therefore been decided to use these connectors from now on for all sensing applications in dusty environments.

5.4.2. FBG evaluation

New developments in the telecommunication and sensing market, have lead to new types of Fiber Bragg Gratings. Three main types can be distinguished: mechanical gratings, UV transparent coated gratings and tower gratings.

5.4.2.1. Mechanical gratings evaluation

The mechanical gratings are the gratings that have been used so far in all the installed FO sensing networks. The process plan for mechanical gratings is shown in Figure 5.6. As input for the process, a coated fiber with a photosensitive core is needed. Two different possibilities exist to get this photosensitivity. The first possibility is to use a high-doped fiber (for example high Ge doping). A disadvantage of this type of fiber is the attenuation (several dB/km) what makes the fiber less interesting for sensing over long distances. The second possibility is using a standard telecom fiber. This fiber has a very low photo sensitivity but can be increased by hydrogenating the fiber prior to FBG writing. For example by putting the fiber for several hours in a hydrogen atmosphere at 150-200 bar at room temperature. After the annealing process the hydrogen is diffusing out and the induced defects (refraction index changes) remain. The use of this type of fiber has the advantage that after annealing a low attenuation can be obtained (<0.5 dB/km) that makes this type of fiber interesting for monitoring over long distances.

In a first step, the coating of the fiber is removed. This is necessary in order not to shield the UV light during the writing of the FBG from the core. Different process technologies are possible: mechanical, chemical, heating or laser removal. Once the coating has been removed, a UV exposure will be performed in order to write the FBG in the core of the fiber. The UV pattern can be applied using the interferometric or the phase mask method. With this method mostly high reflectivity gratings (>90 %) can be produced. The next step is an annealing step. Due to thermal depopulation of trapped states the reflectivity of the grating shows initially a strong decrease. In order to stabilize the grating reflectivity, the FBG is annealed.

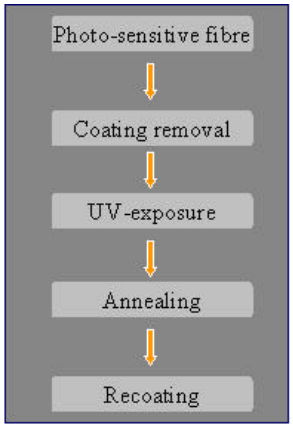

Fig. 5.6: Process steps mechanical gratings

Finally, the fiber will be recoated in order to protect the fiber. Different materials can be used as recoating material like Ormocer, Acrylate, or Polyimde. This type of gratings has been used so far in all applications. The most important disadvantage of the gratings is the low mechanical strength (typically a maximum strain of 1% is the limit). This reduces the reliability of the sensors in case of high strain levels. Higher strain levels can be achieved by some suppliers but due to the special procedure that needs then to be followed, the price almost doubles, making the sensors more expensive.

5.4.2.2. UV-transparent coated fiber gratings

Recently a new type of fiber is introduced on the market: a UV-transparent coated fiber. This fiber does has the advantage that the coating must not be removed prior to UV exposure. As a consequence, the production process becomes simpler, see Figure 5.7. The coating removal as well as the recoating does not need to be performed anymore with this type of fiber. Due to the fact that no stripping has to be applied, the mechanical strength of the fiber is expected to be much better for this type of fiber.

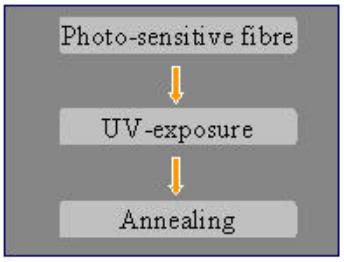

Fig. 5.7: Process steps UV-transparent coated fiber gratings

Due to the interesting high strength properties, this fiber has been put under investigation. A FBG has been written in the fiber after the fiber has been hydrogen loaded. The grating has been written using a wavelength of 248 nm. The writing of a FBG has been successful. A reflectivity around 85% could be obtained. Higher reflectivity's could not be achieved. The reflectivity seemed to saturate around this value.

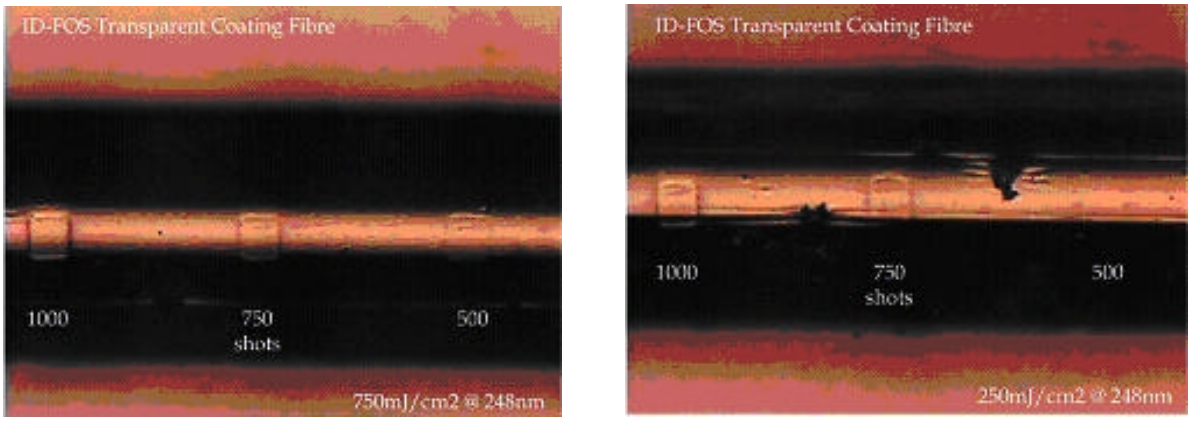

Fig. 5.8: Coating adhesion experiments of UV transparent coated fiber

Furthermore, the quality of the coating has also been analyzed. The coating has been radiated using pulse energies of 250 mJ/cm^2 and 750 mJ/cm^2 and this for 500, 750 and 1000 pulses. After the radiation experiments the coating has been analyzed using a Scanning Electron Microscope (SEM). Figure 5.8 shows the result. As can be observed, ablation effects of the coating did occur even for the smallest dose (250 mJ/cm^2 and 500 shots). This ablation can cause problems with respect to the protection of the fiber. As a consequence, more fine tuning of this type of fiber is required before the fiber can be used in sensing applications.

5.4.2.3. Tower gratings

The tower grating production process is a process that combines the drawing of the fiber and the writing of the FBG. Figure 5.9 shows the set-up of this production process. The input of the process is a pre-form that is used for drawing fibers. The pre-form needs to be highly doped in order to obtain a good photosensitivity of the fiber. By heating the pre-form to 2000 °C, the pulling and formation of the fiber will be initiated. In the way down, the fiber crosses the optical axis of an excimer laser and the interferometer. Using a pulse selector and taking into account the draw speed, FBG's can be written on well-determined places in the fiber. Notice that due to the low available exposure time (15-25 ns), an excimer laser with high pulse energy is used. The gratings will have low reflectivities (<10%). After writing the grating, the fiber will be coated. Finally, the location of the FBG is marked automatically and the fiber is reeled on a drum.

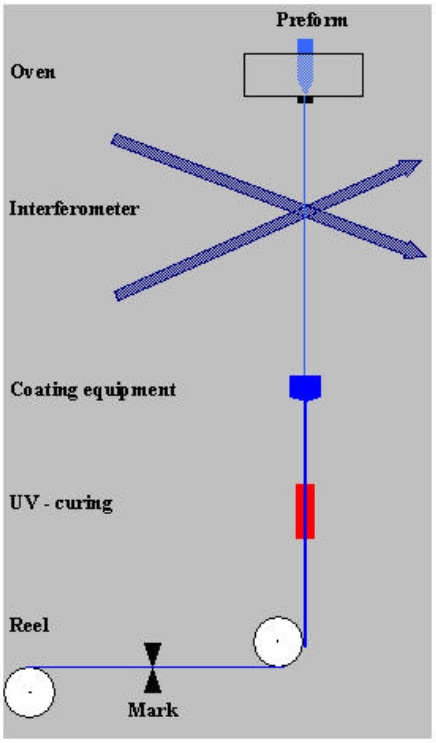

Fig. 5.9: Tower grating production set-up

The advantage of tower gratings is that the FBG is written into the fiber prior to the coating process. As a consequence, no stripping is needed resulting in a good mechanical strength.

Tests have been performed to investigate the mechanical strength of the fiber. Strain levels up to 6% could be obtained without breaking the fiber. This type of fiber is therefore very interesting for future sensors applications.

6. Qualification of sensors, components and network systems

In order to improve the reliability of the Fiber Optical Sensing technology, a first version of a standard and qualification document has been written. The document is focused on FO sensing systems in Nuclear Repository sites. The objectives of this standard are to:

- provide an internationally acceptable standard for general requirements to control, fiber optical sensing systems by defining minimum requirements for design, materials, fabrication, installation, testing, commissioning, operation, maintenance, re-qualification and abandonment
- serve as a technical reference document in contractual matters between purchasers and contractor
- serve as a guideline for designers, purchasers and contractors.

The intention is that the requirements of this document shall apply to all fiber optical sensing systems used in nuclear waste repository sites.

7. Evaluation of results

The overall evaluation of the technical developments have to be performed from different point of views:

1. Sensing capabilities of the developed sensors
2. Sensing capabilities of the interrogating unit: hardware and software.
3. Network efficiency of the whole sensing system

7.1. Sensing capabilities of the developed sensors

7.1.1. Distributed temperature cable

Laboratory investigations and tests on the carbon reinforced fiber can be considered as very successful. An excellent response of the FBGs inside the cable as function of temperature has be observed. The properties of the cable are quite unique due to the low weight and high strength. A first field application is currently performed with this cable at the Mont Terri Underground Research Laboratory in the framework of a heater experiment [29]. Preliminary results are very good.

7.1.2. Fissurometer (mountable strain sensor)

It has been shown that the fissurometer allows monitoring with an extremely high resolution. Calibration results in the lab did show an excellent behavior with respect to linearity and hysteresis. Sensors have been installed in the mine at Morsleben. The results are very good. One advantage of this system in case of long term applications in final repositories is that the sensor can easily be reset for further measurements when the displacement has reached its maximum range. No aging effects have been observed after dismantling of the sensors.

7.1.3. High resolution strain cable

It has been shown that the opto-mechanical cells developed for the strain cable allow measuring displacements with a very high resolution. A very good behavior with respect to linearity and repeatability has been achieved. The in-situ comparison with sliding micrometer measurements in an adjacent borehole had been very helpful in finding remaining shortcomings. The spring mechanism has to be improved especially for serial configuration of interval connections. The temperature effect on the carbon extension cable has to be compensated for. These “learned lessons” have been used to improve the new extensometer configurations recently applied at the Mont Terri and Bure URL in Switzerland and France in the framework of another research project. Within these configurations damping effects are excluded and additional FBGs for temperature measurements have been implemented in each individual carbon cable to compensate for temperature effects [29]. Based on the achieved developments and learned lessons different types of sensing elements can now be made available depending on the kind of application. Each interval in a borehole can be equipped with a different type of sensing element, thus making use of different dynamic ranges and resolutions to optimize the measurement results with regard to the expected deformations.

7.1.4. Porewater pressure sensors

The new design of the porewater pressure sensor has been qualified to measure pressures up to 50 bar within a temperature range between 0 and 180 °C and this with a very good resolution and accuracy. Good results could be obtained for the stainless steel version as well as for the titanium version especially designed for high corrosive environments. Different porewater sensors in stainless steel as well as titanium have been installed at the Äspö URL in Sweden in the framework of a heater test. This test will run for a couple of years and results will be reported in the curse of the corresponding research project.

7.1.5. Total pressure sensors

The new design of the total pressure sensor has been qualified to measure pressures up to 150 bar within a temperature range between 0 and 180 °C and this with a very good resolution and accuracy for the stainless steel version as well as the titanium version. Sensors have been installed at the Äspö URL in Sweden in the framework of a heater test. This test will run for a couple of years and results will be reported in the curse of the corresponding research project.

7.1.6. Humidity sensor

The new calibration algorithm developed for the water leakage sensor has resulted in a much better correlation between the response of the sensor and the actual humidity level. The humidity sensor is reacting very well at different pH levels. No significant influence of pH has been recognized. The used hydrogel showed a resistance to radiation doses up to 1000 Gy. The sensor does show a higher hysteresis for salt solutions than for normal water possibly be attributed to a crystallization of salt in the hydrogel films. The sensor has an 80% R.H. sensitivity threshold. A remaining shortcoming so far is the pressure dependence in case of being embedded in a bentonite material as tested at the GTS, Switzerland, which is not yet being compensated for. Monitoring of slow fluid ingress in terms of dropping rates has been successfully performed at the Morsleben repository.

7.1.7. Hydrogen sensor

The new sensor development with respect to the hydrogen sensor has resulted in a sensor with a high sensitivity. The remaining problem so far is the response time which is currently too slow for the desired application. The third new design that therefore has been taken under development is expected to deal with this problem. However more research is required for fine tuning the production parameters.

7.1.8. PH-sensor

The developed intensity based optical pH sensor did show an excellent behavior for normal short term applications. The results of the field tests at Königstein confirmed the good short term behavior but for the long term drift phenomena have been observed still pending resolution. Possible reasons of this long term drift have been identified. Some more research is required to solve the problem for long term application.

7.2. Sensing capabilities of the interrogating unit

It has been demonstrated that the older interrogation system (FMU-B-SFP) has some shortcomings that might effect the accuracy and reliability of a system for long term applications. The new design of the interrogation system (FMU-B-MOIS) has been tested on lab scale as well as in-situ. It could be shown that the new hardware integration and software development have been performed well. Based on the field tests so far, it can also be concluded that the new system is much more reliable then the FMU-B-SFP.

However, it should be noted that further developments are still required to enhance the reliability even more. As will be explained in the next chapter, recent developments on the telecom and processing market do open new opportunities to enhance reliability and accuracy and to lower the cost of the interrogation systems even more. Especially the introduction of MEMS (Micro Electro-Mechanical) devices opens a complete new view on interrogation systems with respective to performances, dimensions and cost.

7.3. Network efficiency of a whole sensing system

7.3.1. Multiplexing

The wavelength domain multiplexing has proven its reliability in the laboratory as well as in the field trials. The multiplexing possibilities have been extended due to the development of the series configuration set-up for the pressure sensors.

In the past, efforts had been put into the development and design of optical switches. It looks now that this is not a good economical solution anymore. A lot of suppliers can be found in the telecom market providing switches on a relative low cost and with excellent specifications like lifetime, reliability, and optical losses.

7.3.2. Cabling and connectors

For optical links out of boreholes, normal outdoor telecom cables have been safely and easily implemented at different test sites. This shows that the sensing network can be build using very standard cables of a mass production industry (telecom) i.e. very cost effective cables.

No problem encountered with the cabling techniques so far. The cabling of the network has been reduced to fibers blown into nylon 6/3mm tubing usually used for pneumatic and hydraulic sensors. Theses tubing provide the solution for cabling grouted sensors since they withstand high (grout) pressure while being cost effective.

With respect to the connectorization, the new connectors that have been used (E2000 series) show a significant improvement with respect to contamination and signal transmission.

7.3.3. Long term behavior

The oldest test installation (Konrad Mine) did show a very good correspondence between conventional and the fiber optical sensors. The test equipment was dismantled in June 2003. The sensors had been taken back to the laboratory for further investigation. The results did show that the sensor response is still excellent, no aging effects and no visible contamination of the inner parts were present. This subscribes the long term monitoring capabilities and reliability of fiber optic systems.

8. Outlook on future developments

In the following subchapters a brief description of future development options is given. These options include

- new pH sensing systems
- smart geotextiles with optical fibers
- wireless data-logging systems for optical monitoring systems
- improvement of optical hydrogen sensing

8.1. Development of pH sensing fiber based on FBG technology

The current state of the intensity based fiber optical pH sensor (as described in 4.10) did show some shortcomings. A drift effect has been observed. A possible reason is the ageing of the LED. In order to circumvent these intensity based problems it is proposed to develop a pH-sensor based on FBG-technology. Three different types are here proposed. With the first two sensors, the FBG is used to measure the changes in refraction index of a pH sensitive chemical layer. With the third sensor, a material will be used that will swell as function of pH. This swelling will be recorded using a FBG. All three principles do have the advantage that different sensors can be put in series what allows to monitor multiple sensing points on one optical line.

8.1.1. pH sensor type 1: Side polished FBG refractometer

Beside the influence of temperature and strain on the Bragg wavelength of a FBG, the effective refractive index of the guided fiber mode can respond also to changes in the refractive index of the material within the evanescent field region. This effect has been demonstrated in previous reports using etched D-shaped fiber [16], uniformly etched fiber [17], and long-period gratings [18, 19].

Applying the so-called polished fiber half-coupler technology to fiber segments containing in-fiber Bragg gratings results in mechanically stable fiber-optic structure with the possibility to expose evanescent field of the FBG to an analyte.

Sensor type 1 will be based on this principle. Figure 8.1 shows the schematic design of the sensor. The sensor consists of a single-mode fiber embedded in a fused silica block that will be polished to the proximity (<0.5 µm) of the fiber core. One FBG will be inscribed into the fiber core using an interferometric arrangement in the central sensing region (measuring grating). For comparative measurement of temperature influences, a second FBG will be inscribed in the deeper embedded fiber core region with no accessible evanescent field of the fiber mode. On top of the FBG at the centre of the polished surface, an analyte will be deposited that has a pH sensitive refraction index. This refraction index will be measured using the response of the FBG due to the evanescent field interaction of the guided fiber mode. Since the disturbance is not symmetric around the fiber, the FBG response will be strongly dependent on the polarization mode of the light.

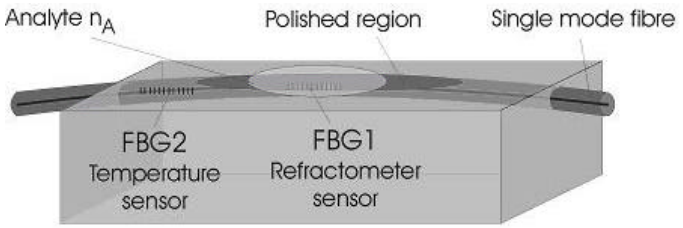

Fig. 8.1:
Schematic of the sensor head with two fibre Bragg gratings: - Refractometric sensor FBG1 in side-polished fibre; - Temperature reference sensor FBG2.

8.1.2. pH Sensor type 2: Micro-machined FBG refractometer

The second type of sensor makes also use of influencing the evanescent field interaction of the guided fiber mode through a fiber bragg grating. In order to get to the evanescent field, the cladding at the position of an FBG will be removed in a rectangular shape by using a vacuum UV laser micro machining technology. Figure 8.2 shows an example of a micro-machined fiber (SMF-28). The etched region will be filled with a pH sensitive analyte which refraction index can be measured using the FBG response.

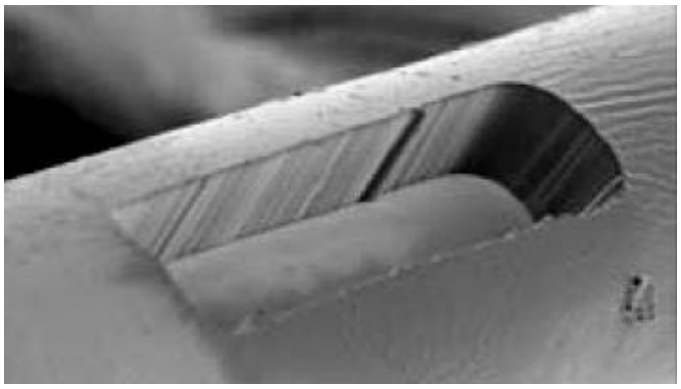

Fig. 8.2:
Micro machined SMF-28 fiber of corning using a F_2 laser.

8.1.3. pH sensor type 3: Strain based FBG pH-sensor

The design of sensor type 3 is shown in Figure 8.3. The sensor makes use of the strain sensitivity of the grating. The sensor consists of a grating that locally will be etched in order to reduce the cladding on the position of the grating. As a consequence the stiffness of the fiber becomes smaller and the grating will show a higher strain response as function of an external force. The cladding in the direct neighborhood of the core will not be etched in order not to create evanescent field effects as is the case with the previous two sensors. In a second step the etched region will be recoated with a chemical layer that shows a swelling effect as function of the pH value. Due to the swelling the grating will be strained and a wavelength shift will be observed.

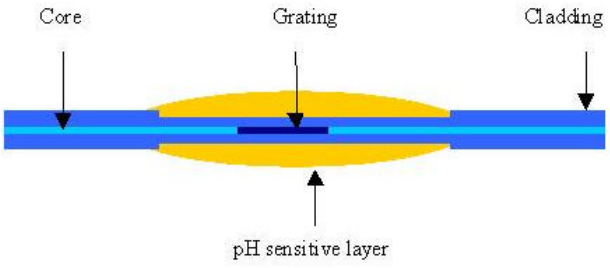

Fig. 8.3: Schematic design strain based pH-sensor

8.2. Reinforcement and monitoring of tunnel walls using smart geotextiles

A smart geotextile has currently been developed. The smart geotextile is a reinforcement carpet that has been equipped with fiber optical strain sensors to measure the settlement of the structures.

Figure 8.4a shows a sample of the smart geotextile carpet with 1 optical fiber line inside. The optical fiber is equipped with a yellow coating to prevent water intrusion and to make handling easier. The geotextile is a non-woven carpet. This is reinforced by polypropylene fiber bundles (white horizontal lines). These reinforcement bundles are sewed onto the geotextile, where the needle is not sewing into the reinforcement bundle (see Fig. 8.4b). This is very important because some polypropylene fibers are replaced by the yellow coated optical fiber.

Vertical sewing is performed, to keep everything better on its place. This gives the typical raster structure as can be seen in figure 8.4a.

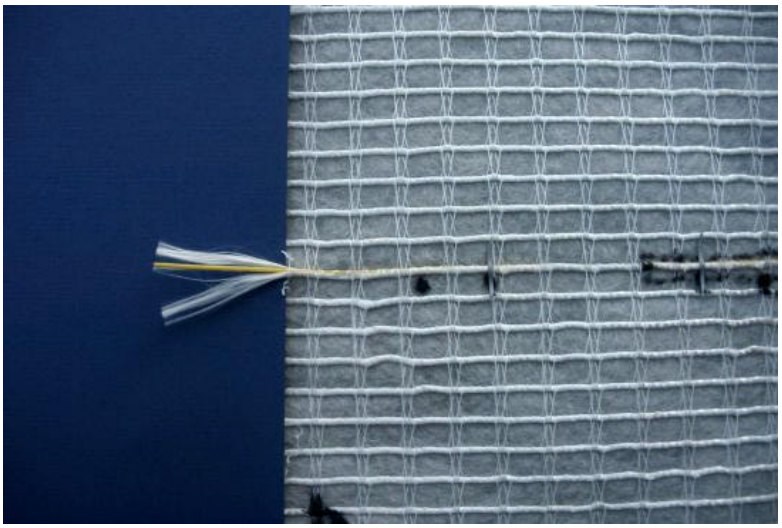

a)

b)

Fig. 8.4:

a) Sample smart geotextile carpet

b) Sewing principle of reinforcement bundles

Figure 8.5 shows an application example for these geotextile carpets. The geotextile is here used for the reinforcement of the soil. When a deformation of the underground occurs in the form of a void, the geotextile will deflect and induce a counterforce. The deflection results also in an increased strain on the fiber optical sensors. As a consequence the magnitude of deflection (deformation) is continuously monitored. A similar principle can be used for tunnel wall reinforcement. This needs however to be investigated in much more detail.

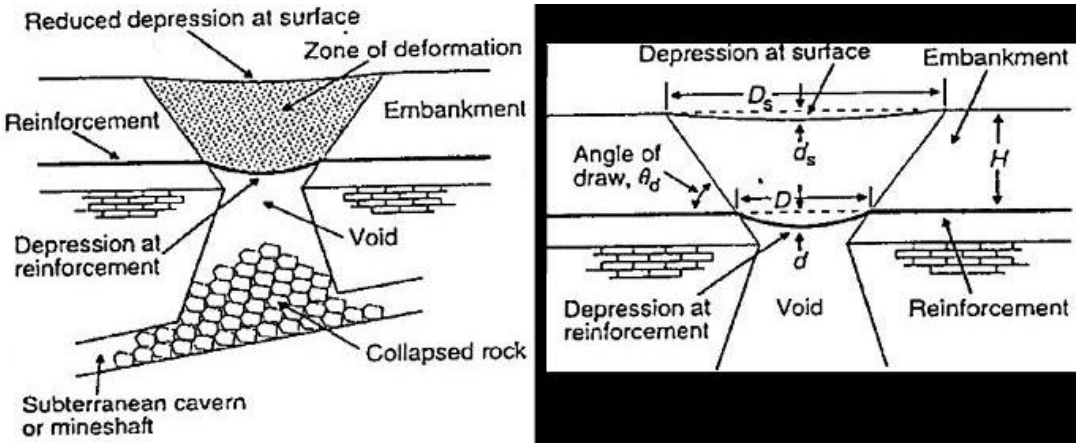

Fig. 8.5: Application example of smart geotextiles

8.3. Development wireless FBG-datalogging system

An important and critical part with respect to cost and reliability of the FBG-sensing technology is the interrogation system. So far, all interrogation systems have been based on expensive benchtop models that are controlled using a laptop or desktop PC. Due to this combination, the systems are not very ruggedised and less reliable then a complete integrated system.

It is therefore proposed to develop a complete stand-alone integrated system that has the following properties:

1. Accurate wavelength determination with high resolution
2. Processing and saving capabilities
3. Interrogation of different optical lines (Optical switch)
4. Extended measurement range: C+L band
5. Extended interfacing: Ethernet, RS232, USB
6. Wireless access using RF-signals
7. Compact dimensions
8. Relative low cost price
9. High reliability

This can now be achieved due to some recent developments in the telecom and embedded system market such as:

- The developments of the MEMS technology in the telecommunication market. MEMS stands for Micro Electro Mechanical Systems. These systems are manufactured using complete automatic processes which result in a drastic cost decrease of the components. The MEMS products are also very compact. So far, tunable MEMS filters as well as optical MEMS switches have been developed with specifications exceeding or comparable to the conventional filters and switches.
- The recent development of high resolution calibration cells. These cells make use of well determined gasses with absorption characteristics in the C-band. The temperature dependence of these cells is even much lower than the 'picowave' reference module from Micron Optics. A much better accuracy is therefore expected.
- The recent development of low cost embedded processors which can perform complex functions. The control of the filter as well as the processing of the data can be performed using these systems.
- Development of low cost C and L-band SLED's (super light emitting diodes).

Finally, it needs to be noticed that the wireless property is giving a very important added value to the system. Sensing network configurations becomes much more flexible and can be positioned at difficult or non accessible places.

8.4. Further development of hydrogen sensor

As explained above, a new design for the hydrogen sensor has been proposed. The sensor consist of a naked FBG that will be recoated using Pd. It needs to be noticed that this design is very promising concerning response time due to the thin Pd layer that is used to strain the FBG.

First tests with this method did show some problems with respect to stress build up between the Pd and the used glass substrate. However, some solution for these problems do exist such as the use of intermediate buffer layers (example Ti). However, more developments are required to find the optimum process parameters.

9. Final conclusions

The main deliveries of the project listed in the introduction are:

1. Development of new sensors addressing the agreed parameters such as: pH, hydrogen, distributed temperature, porewater pressure, total pressure, fissurization, and high resolution deformation effects.
2. Further development and improvement of the interrogation systems for monitoring of complex large scale sensing networks.
3. Extending the evaluation results of the behavior of the fiber optical monitoring systems in real field installations.

The selected sensors have all been developed and validated. Some sensors still require some more fine tuning but the overall goal has been achieved.

The interrogation system has completely be redesigned and improved with respect to accuracy and reliability.

A couple of field installations have been equipped during the project for evaluating and qualifying the developed fiber optical sensing network systems. A good correspondence with conventional sensors has been demonstrated. After dismantling of the sensing network at the Konrad site, all sensors had been recalibrated and did still show an excellent sensor response. No contamination or malfunctioning could be observed after almost 4 years of operation.

From all these field results it can be concluded that fiber optic monitoring systems devoted to operational safety in nuclear waste disposal sites is becoming a very interesting alternative for the conventional electrical sensing systems.

In order to bring these fiber optical sensing systems closer to a commercialization level, a draft of a standard and qualification document for applying fiber optic sensing systems in nuclear waste repository sites has been written.

Finally, it should be mentioned that new developments have been proposed to extend the possibilities and reliability of the fiber optic sensing systems. The net result of the R&D achievements of the project and of its follow up R&D trends will be a high performance global self-operating long term monitoring system for final disposal sites.

10. References

[1] *Engelmann, H.-J., Jobmann, M., Voet, M. 1995:* Study of electro-optical sensing systems for long term monitoring at underground nuclear waste disposal sites, Final Report, DBE, Peine.

[2] *Jobmann, M., Fischer, S., Voet, M. 2000:* Development and test of redundant fiber optic sensing systems with self operating control for monitoring at final disposal sites, Final Report, DBE, Peine.

[3] *Jobmann, M., Fischer, S., Voet, M. 2000:* New monitoring methods for operational safety requirements based on fiber optic technology, Proceedings of the International Conference on Radioactive Waste Disposal - DisTec-2000, Berlin.

[4] *Ferdinant, P. et. al, 1994*: Mine operating accurate STABILity control with Optical fiber Sensing and bragg grating technology: BRITE-EURAM STABILOS project, Optical Fiber Sensor Conference OFS (10), Glasgow.

[5] *Othonos, A., Kalli, K. 1999*: Fiber Bragg Gratings - Fundamentals and application in telecommunications and sensing, Artech House Publishers, Boston, London.

[6] *Culshaw, B., Dakin, J. 1989*: Optical Fiber Sensors, Volume 1, Artech House Publishers, Boston, London.

[7] *Jobmann, Michael 2002*: Faseroptische Mess-Systeme und ihre Einsatzmöglichkeiten im Bereich der Endlagerung, atw 47, Heft 6, Berlin.

[8] *Jobmann, M., Biurrun, E. 2003*: Research on Fiber Optic Sensing Systems and their Application as Finals Repository Monitoring Tools, Proceedings of the WM'03 Conference, February 23-27, 2003, Tucson, USA.

[9] *Jobmann, M., Kranz, H., Biurrun, E. 2003*: Fiber Optic Sensing Systems and their Possible Application as Safeguards Monitoring Tools, Proceedings of the 25th ESARDA Symposium, Stockholm.

[10] *Johnson, G.*: LabVIEW Graphical programming; ISBN 00703291.

[11] *Johnson,G.*: LabVIEW Power programming; ISBN 0079136664.

[12] *Wells*: LabVIEW for Everyone: Graphical programming made even easier, ISBN 0132681943.

[13] *Eriksson, M., Ekedahl, L.G. 1997:* Sensors and actuators B42, pp. 217.

[14] *Ratajczykowa, I., 1986*: Surface Science 172, pp. 691.

[15] *Peng, Y.T., Tang, Y., Sirkis, J.S. 1999*: Hydrogen Sensors Based on Palladium Electroplated Fiber Bragg Grating (FBG), Proceedings OFS-13, Kyongju, Korea.

[16] *Meltz, G., Hewlett, S.J., and Love, J.D. 1996*: "Fiber grating evanescent-wave sensors", Proceedings of SPIE, Vol. 2836 Chemical, Biochemical, and Environmental Fiber Sensors VIII, pp 342.

[17] *Asseh, A., Sandgren, S., Ahlfeldt, H., Sahlgren, B., Stubbe, R., and Edwall, G. 1998*: "Fiber optical Bragg grating refractometer", Fiber and Integrated Optics, Vol. 17, pp 51.

[18] *Falciai, R., Mignani, A.G., and Vannini, A. 1998*: "Solution concentration measurements by means of optical fiber long-period gratings", Proceedings of SPIE, Vol. 3483: European Workshop on Optical Fiber Sensors, pp 95.

[19] *Patrick, H.J., Kersey, A.D., and Bucholtz, F. 1999*: "Analysis of the response of long period fiber gratings to external index of refraction", Journal of Lightwave Technology, Vol. 16, no. 9, pp 1606.

[20] *Tang, et al. 1999*: Characterization of Fiber Bragg Grating (FBG) Based Palladium Tube Hydrogen, Proceedings of OFS-13, Kyongju, Korea.

[21] *Bévenot, X., Trouillet, A., Veillas, C. and Gagnaire, H. 2000*: Sensors and Actuators B67, pp. 57.

[22] *Butler, M.A. and Bus, R.J., 1993*: Sensors and Actuators B, 11 p. 161.

[23] *Mueller W.M., Blackledge J.P., Libowitz G.G., 1968*: Metal hydrides, Academic New York.

[24] *Eriksson, M., Ekedahl, L.G. 1998*: Applied Surface Science 133 p. 89.

[25] *Kiskinova, M.P., Bliznakov, G.M. 1982*: Surface Science 123 p. 61.

[26] *Kok, G.A., Noordemeer, A., Nieuwenhuys, B.E. 1983*: Surface Science 135 p. 65.

[27] *Baldini, F. 1998:* Optical determination of pH with optical fibers, Trends in Applied Spectroscopy, Vol. 2, pp. 119-128.

[28] *Baldini, F. 1998:* Critical review of pH sensing with optical fibers, SPIE Conference on Chemical, Biochemical, and Environmental Fiber Sensors X, Boston, Massachusetts, SPIE Vol. 3540.

[29] Polster, M., Schonebeck, M., Jobmann, M. 2005: Investigation on thermal expansion effects in clay formations, F+E-Vorhaben TEE, Jahresbericht 2004, DBE TECHNOLOGY, Peine.

[30] Schonebeck, M., Jobmann, M. 2005: Investigation on the THM behavior of a heated bentonite barrier by measurements and numerical calculations, F+E-Vorhaben Muster, Annual Report 2004, DBE TECHNOLOGY, Peine.